OFFICE OF climate change
Queensland Climate Change Centre of Excellence
Research Report

Department of Environment and Resource Management

Rainfall in Queensland

Part 4: The ability of HiGEM to simulate Queensland's rainfall variability and its drivers

Prepared by Nicholas Klingaman

February 2012

Walker INSTITUTE

National Centre for Atmospheric Science
NATURAL ENVIRONMENT RESEARCH COUNCIL

Toward Tomorrow's Queensland

Queensland Government

Prepared by:

Nicholas P. Klingaman, Walker Institute for Queensland Climate Change Centre of Excellence,

Department of Environment and Resource Management

GPO Box 2454

Brisbane Qld 4001

ISBN 978-0-9805641-1-2

Disclaimer

This document has been prepared with all due diligence and care, based on the best available information at the time of publication. The department holds no responsibility for any errors or omissions within this document. Any decisions made by other parties based on this document are solely the responsibility of those parties. Information contained in this document is from a number of sources and, as such, does not necessarily represent government or departmental policy.

If you need to access this document in a language other than English, please call the Translating and Interpreting Service (TIS National) on 131 450 and ask them to telephone Library Services on +61 7 3224 8412.

This publication can be made available in an alternative format (e.g. large print or audiotape) on request for people with vision impairment; phone +61 7 3224 8412 or email <library@derm.qld.gov.au>.

Citation:

Klingaman, N.P., 2012: The ability of HiGEM to simulate Queensland's rainfall variability and its drivers. QCCCE Research Report: Rainfall in Queensland. Part. 4. Department of Environment and Resource Management, Queensland Government, Brisbane, Australia. Available online at www.derm.qld.gov.au.

To contact the author:
E-mail: n.p.klingaman@reading.ac.uk
Post: Department of Meteorology
University of Reading
Earley Gate, P.O. Box 243
Reading, Berkshire RG6 6BB
United Kingdom

Acknowledgements

Dr Nicholas Klingaman was funded by a grant from the Queensland Government, under a collaboration between the Queensland Climate Change Centre of Excellence (QCCCE) and the Walker Institute for Climate System Research at the University of Reading (http://www.walker-institute.ac.uk). Dr Klingaman was supervised by Steve Woolnough of the Walker Institute and Jozef Syktus of QCCCE. Dr Klingaman acknowledges productive discussions with Ken Day of QCCCE.

SILO rainfall data were provided by the Queensland Government. 20th Century Reanalysis V2 data were provided by the NOAA/OAR/ESRL PSD, Boulder, Colorado, USA, from their Web site at http://www.esrl.noaa.gov/psd/. Support for the Twentieth Century Reanalysis Project dataset is provided by the U.S. Department of Energy, Office of Science Innovative and Novel Computational Impact on Theory and Experiment (DOE INCITE) program, and Office of Biological and Environmental Research (BER), and by the National Oceanic and Atmospheric Administration Climate Program Office. HadISST SSTs were provided by the British Atmospheric Data Centre, under agreement with the U.K. Met Office. IBTrACS data were provided by the U.S. National Climatic Data Centre. HiGEM model output data were provided by the National Centre for Atmospheric Science in the United Kingdom.

Published February 2012

Contents

List of figures

List of tables

1 Executive Summary

Stakeholders and policymakers are seeking detailed information on the impacts of climate change and variability, especially on rainfall, at the local and regional levels. This information can be delivered by only those global climate models that represent the atmosphere and ocean at fine resolution, to robustly simulate the weather systems that produce rainfall. These models provide us with a better understanding of the key meteorological phenomena that affect Queensland. That knowledge can then be used to improve the simulation of these phenomena in lower-resolution climate models. Implementing these improvements will provide more accurate predictions on weekly to seasonal and decadal timescales, as well as more robust predictions of the impacts of climate change on these phenomena.

High-resolution Global Environment Model, version 1.1 (HiGEM) is a global, coupled climate model that was developed by the U.K. academic community. It is based on the U.K. Hadley Centre's HadGEM1 model, but HiGEM has considerably higher resolution: 90 km in the atmosphere and 30 km in the ocean. HiGEM has been used in this research as its increased resolution may allow the model to better represent regional climate variability and change in Queensland.

In this research, a 150 year control simulation of HiGEM was assessed to evalute the ability of the model to simulate Queensland's rainfall and its inter-annual and decadal variability. HiGEM was also assessed for its ability to produce the observed Empirical Orthogonal Teleconnection (EOT) patterns of rainfall avariability obtained from the SILO gridded rainfall dataset.

In the mean, HiGEM produces less rainfall over Queensland than observed, particularly in the north of the state. Most of this dry bias occurs because the model simulates a weaker Australian summer monsoon than is observed. However, HiGEM represents well the relationship between the El Niño Southern Oscillation (ENSO) and Queensland rainfall, on annual and seasonal timescales. The model even captured the observed asymmetric correlation between the ENSO and Queensland rainfall: stronger La Niña events cause stronger flood years in Queensland, but stronger El Niño events do not cause stronger droughts.

The research found that HiGEM lacks the ability to model decadal variations in Queensland rainfall and in the teleconnection between the ENSO and rainfall. This is likely due to the model's inability to simulate the Interdecadal Pacific Oscillation (IPO), which has been identified as the key driver of these variations.

In relation to the generation of tropical cyclones, HiGEM captures the observed regions of tropical-cyclone formation and the correct distributions of tropical cyclone tracks, but simulates too many tropical cyclones in the Southwest Pacific.

When EOT analysis is applied to HiGEM and the results are compared with the EOT patterns computed using observed rainfall, HiGEM performs well for those EOTs related to the ENSO in summer, winter and spring. HiGEM also represents the relationship between Southeast Queensland rainfall and onshore easterly winds, including the decadal variations in the winds' strength and moisture content. Futher, HiGEM correctly simulates the observed association between the frequency of tropical cyclones and summer rainfall in Cape York.

The success of HiGEM at reproducing many of the observed EOTs, particularly in summer, increases our confidence in the model's ability to predict the impact of climate change on Queensland's rainfall and its drivers.

2 Introduction and objectives

There is considerable uncertainty in projections of rainfall changes in Australia in a warmer world. Suppiah et al. (2007) demonstrated that the coupled climate models that contributed to the Intergovernmental Panel on Climate Change (IPCC) Fourth Assessment Report (AR4) produced a wide range of projected rainfall changes, extending from a 20 per cent increase per degree Celsius of global-mean warming to a 20 per cent decrease per degree Celsius. As global temperatures may increase by 2 degrees Celsius over the next fifty years, this uncertainty is considerable and limits the ability of society to successfully adapt to climate change. The uncertainty concerning how climate change will affect modes of inter-annual and decadal climate variability, such as the El Niño–Southern Oscillation (ENSO), is still greater.

As these modes of variability influence the frequency and intensity of rain-bearing weather systems such as tropical cyclones (e.g. Walsh and Syktus 2003) and east-coast cyclones (e.g. Hopkins and Holland 1997), the impacts of climate change on the spatial and temporal characteristics of rainfall may be considerably more uncertain than the change in the mean. Further, many of the climate models used for AR4 had horizontal grids too coarse to resolve these rain-bearing systems well, highlighting the need for finer-resolution coupled models. Suppiah et al. (2007) found that many models also displayed considerable biases in Australian temperature and rainfall in their "control" simulations with pre-industrial levels of carbon dioxide, although it is unclear whether such biases should necessarily hamper a model's ability to accurately simulate the response of the Australian climate to increased levels of carbon dioxide.

The Fifth Coupled Model Intercomparison Project (CMIP5) includes not only centennial climate-change simulations, but also a series of initialized decadal hindcasts and predictions (Taylor et al. 2009). The hindcasts will assess coupled models' ability to simulate the evolution of the climate system since 1960, while the predictions aim to improve understanding of the impacts of climate change over the next 10–30 years. The U.K. High-resolution Global Environment Model (HiGEM) is contributing to this decadal prediction experiment, using horizontal resolutions in the atmosphere and ocean much finer than the coupled models used for AR4 (Section 2.1). Such resolutions raise the prospect of more accurate simulations of regional-scale climate variability and change. Previous analysis of HiGEM has shown, for example, that its fine resolution improves the simulation of the ENSO, which is a key driver of Queensland's rainfall. The HiGEM CMIP5 decadal integrations therefore hold considerable promise for increased understanding of the predictability of Queensland's rainfall on timescales of 1–10 years.

Before undertaking analysis of the HiGEM CMIP5 decadal hindcasts and predictions, however, it is necessary to conduct a thorough evaluation of the model's ability to simulate Queensland's rainfall, its inter-annual and decadal variability and its relationship with known synoptic and climate drivers, such as the ENSO. This report builds upon the knowledge gained and techniques applied in Klingaman (2012a)—a summary of previous research into drivers of Queensland's rainfall—and Klingaman (2012b)—a detailed analysis of the drivers of state-wide and regional variations in seasonal rainfall in Queensland, as well as how the strengths of those drivers have changed over time.

In this report, the 150 year HiGEM control simulation is analysed in terms of Queensland's rainfall and its drivers. Section 2 describes HiGEM, the data to which the model is compared, and the method of empirical orthogonal teleconnection (EOT) analysis used to decompose the seasonal Queensland rainfall from HiGEM into patterns of coherent variability. Section 3 discusses the climatology and inter-annual and decadal variability of seasonal- and annual-mean Australian rainfall in HiGEM. The ability of HiGEM to simulate key drivers of Queensland rainfall, including ENSO and the Interdecadal Pacific Oscillation (IPO), is assessed in Section 4. The EOTs of seasonal HiGEM rainfall are compared to those computed from the SILO gridded analyses (Klingaman 2012b) in Section 5, to reveal which physical mechanisms underlying Queensland rainfall are robustly simulated in HiGEM and which are not.

3 Data and methods

3.1 HiGEM control simulation

This report analyses the output from a 150 year pre-industrial control simulation of the U.K. High-resolution Global Environment Model, version 1.1 (HiGEM) coupled atmosphere–ocean general circulation model (Shaffrey and others, 2009). HiGEM is a finer-resolution version of the Hadley Centre Global Environmental Model (HadGEM1; Ringer et al. 2006). In HadGEM1, the atmospheric and oceanic horizontal resolutions are 1.875° longitude × 1.25° latitude and 1° longitude × 1° latitude (refining to 0.33° latitude near the equator), respectively; in HiGEM these are 1.25° longitude × 0.83° latitude and 0.33° longitude × 0.33°, respectively. Both models have 38 (40) vertical grid points in the atmosphere (ocean). Numerous changes to the HadGEM1 physical parameterizations were made in HiGEM, which will not be discussed here; Shaffrey and others (2009) contains details of these.

For the atmosphere and land surface, the HiGEM control simulation was initialized from a European Centre for Medium-range Weather Forecasts (ECMWF) analysis. Ocean potential temperatures and salinities were set to September values from the World Ocean Atlas (Conkright et al. 2002); ocean currents were initialized at rest. The first several decades of the coupled control integration are therefore likely to be affected by the adjustment of the HiGEM ocean towards an equilibrium state. As in Shaffrey and others (2009), we discard the first 20 years of the integration and base our analysis on years 21–150 only.

Shaffrey and others (2009) and Roberts and others (2009) demonstrated that the finer atmospheric and oceanic resolutions in HiGEM considerably improved many aspects of the mean climate and inter-annual variability over HadGEM1. Most importantly for Queensland, relative to HadGEM1, HiGEM has a reduced dry bias over northern Queensland (Shaffrey et al. 2009, Fig. 6), a reduced easterly 850 hPa wind bias (Shaffrey et al. 2009, Fig. 10) and a more realistic spatial and temporal pattern of sea-surface temperature (SST) variability associated with the ENSO (Shaffrey et al. 2009, Figs. 19 and 20). The latter is linked to an improved simulation of the Pacific mean state in both SSTs and atmospheric circulation, which Roberts and others (2009) demonstrated was due in large part to HiGEM's ability to resolve tropical instability waves.

3.2 SILO gridded rainfall analyses

Means and inter-annual and decadal variability of seasonal and annual rainfall across Queensland were taken from the SILO dataset of kriged gauge values (Jeffrey 2001) on a 25 kilometre grid for the period March 1900–February 2008. Before comparing against HiGEM, the SILO data were linearly interpolated onto the HiGEM horizontal grid (Section 2.1) using an area-weighted method. Jeffrey (2001) used cross-validation to show that the monthly SILO totals were reliable across most of Queensland, with particular skill in coastal regions with high station densities, but were less skilful in the far north of the Cape York Peninsula where there are few stations with long records.

3.3 TRMM gridded rainfall analyses

As SILO covers only land points, seasonal and annual climatological precipitation from the Tropical Rainfall Measuring Mission (TRMM; product 3B42, version 6A) is used to evaluate climatological rainfall in HiGEM over the oceans surrounding Australia. TRMM data were available for 1999–2010 on a 25 kilometre grid. This record is substantially shorter than either SILO or the HiGEM control integration, but alternative products with longer records (e.g. from the Centre for Merged Analysis of Precipitation (CMAP)) either provide much coarser spatial resolution (e.g. 2.5° for CMAP) or do not provide continuous global coverage. TRMM is used only to determine biases in the HiGEM climatology over the oceans around Australia; all analysis of inter-annual and decadal variability uses SILO rainfall only. Once SILO and TRMM were interpolated to the HiGEM horizontal grid, the products were combined using the HiGEM land–sea mask: SILO at points that HiGEM considers land or fractionally land (i.e. "coastal tiled" points, see Shaffrey et al. (2009)); TRMM at points that HiGEM considers ocean.

3.4 HadISST sea-surface temperatures

Monthly-mean, 1900–2007 SSTs from the 1° × 1° Hadley Centre Sea Ice and SST dataset (HadISST; Rayner et al. 2003) are used to compute observed decadal variability in Pacific SSTs, for comparison with HiGEM. The observed Inter-decadal Pacific Oscillation (IPO) is calculated by the method of Folland et al. (1999) and Arblaster et al. (2002), which uses empirical orthogonal functions (EOFs) of 13 year lowpass-filtered seasonal-mean SSTs between 40°S–60°N.

3.5 HadCM3 control simulation

Pacific decadal variability in HadISST and HiGEM is compared to that from the 1000 year control integration of the Hadley Centre coupled model, version 3 (HadCM3; Gordon et al. 2000). The IPO in HiGEM is identified using the EOF technique described in section 2.4 above. For consistency with the 150 year HiGEM control integration, both the total decadal SST variability and the IPO are computed from consecutive 150 year periods in HadCM3, beginning with year 101 (e.g. years 101–250, years 251–400). Decadal variability in HiGEM, HadCM3 and HadISST is analysed in Section 4.2.

3.6 Tropical cyclone tracks

Observed tropical cyclone tracks for the South Pacific basin were obtained from the International Best Track Archive for Climate Stewardship (IBTrACS; Knapp et al. 2010) for October–May seasons during 1950–2008. Although observational coverage of the basin was limited prior to the satellite era, this longer period is chosen for better correspondence with the 130 years of the HiGEM control integration. To generate statistics of tropical-cyclone activity such as track, genesis and lysis densities on a regular grid, the IBTrACS tracks were processed by the method of Hodges (1996). Cyclone densities are expressed in units of storms per season within a 5° radius spherical cap of each T62 (approximately 1.9° longitude × 1.9° latitude) grid point; the unit area is approximately equal to 10^6 kilometre squared.

Tropical cyclone tracks from HiGEM were detected by the method of Thorncroft and Hodges (2001), in which tropical and extra-tropical cyclones are separated by their vertical structure: cyclones must display a warm-core structure and must attain a near-surface 20 meters per second wind speed before being classified as "tropical". Cyclone statistics from HiGEM were obtained from tracks in precisely the same manner as for IBTrACS, using October–May as the tropical-cyclone season in the South Pacific. It is important to note that cyclones in HiGEM continue to be tracked after they become extra-tropical, while the extra-tropical parts of the cyclone track are not included in the IBTrACS statistics. This leads to considerably longer tracks in HiGEM, as well as variations in cyclone lysis locations; the impacts of this will be discussed in Section 4.3.

3.7 Empirical orthogonal teleconnection analysis

Empirical orthogonal teleconnection (EOT) analysis is used to determine whether HiGEM is able to represent the influences of observed atmospheric drivers on inter-annual and decadal Queensland rainfall variability. EOT analysis was performed on seasonal-mean Queensland rainfall, using an identical procedure to that employed by Klingaman (2012b) on the SILO dataset for Queensland and by Smith (2004) on rainfall across Australia. The first six EOTs from HiGEM were computed for each three-month season: December–February (DJF), March–May (MAM), June–August (JJA) and September–November (SON). While Klingaman (2012b) analysed only the first three EOTs from SILO, the first six EOTs were computed for HiGEM to increase the probability of finding a HiGEM EOT that closely matched one of the three leading SILO EOTs. None of the fifth or sixth HiGEM EOTs matched any of the first three SILO EOTs, however, so only the four leading HiGEM EOTs are considered further.

The four leading HiGEM seasonal EOTs, the fraction of the variance in the HiGEM area-averaged Queensland rainfall that each explains, and correlations with various indices of atmospheric drivers are given in Table 1, which is printed near the discussion of the EOTs and their drivers (Section 5) for ease of reference. This table is similar to Table 1 from Klingaman (2012b)—reproduced in Appendix A (Table 3)—with one notable difference: the HiGEM table contains no correlations between the EOTs and the Inter-decadal Pacific Oscillation (IPO). The reasons for this are given in Section 4.2.

To identify the atmospheric driver of each HiGEM EOT and make comparisons with the observed drivers from Klingaman (2012b), regressions of each HiGEM EOT onto HiGEM seasonal-mean mean sea-level pressure (MSLP), 850 hPa zonal and meridional wind (u850 and v850), 500 hPa zonal and meridional wind and specific humidity (u500 ,v500 and q500) and SST are performed. Regressions of each EOT onto the seasonal standard deviations in HiGEM 2–10 day bandpass-filtered MSLP (MSLP2–10d) are used to identify anomalies in synoptic activity. While regressions of all four EOTs against all fields were performed, only those regressions relevant to each identified driver will be shown.

4 Queensland rainfall in HiGEM and its inter-annual and decadal variability

HiGEM shows consistent mean-state dry biases over northern and eastern Queensland, with wet biases just offshore (Fig. 1c). The biases are roughly proportional to the seasonal-mean rainfall, with DJF (Fig. 1f) and MAM (Fig. 1i) displaying much greater errors than JJA (Fig. 1l) and SON (Fig. 1o). These biases are not due to the use of different climatologies for land (SILO) and ocean (TRMM) grid points, as the SILO and TRMM annual-mean (Fig. 2) and seasonal-mean (not shown) climatologies are remarkably similar over Australian land points, except that SILO is slightly drier than TRMM across northern Queensland. Rather, HiGEM generates too much precipitation over the ocean, draining moisture out of the air before it reaches land and leading to dry biases. This pattern of biases may be due to the "coastal tiling" scheme in HiGEM, in which small fractions of near-coastal grid points that would ordinarily be entirely ocean are instead assigned the surface properties of land grid points. The scheme is designed to smooth the transition between land and ocean in the model, but it results in the atmospheric circulation responding to the coastline prior to the flow reaching the continent, which may lead to rising motion and precipitation over the ocean instead of over land.

To assess the inter-annual variability in rainfall in HiGEM, the normalized inter-annual standard deviations are computed for HiGEM and SILO: at each grid point, the HiGEM or SILO inter-annual standard deviation is divided by the HiGEM or SILO climatological rainfall. The ratios of these normalized standard deviations evaluate whether, for its own climatology, HiGEM has the same level of variance on inter-annual temporal scales as the SILO analyses. HiGEM performs relatively well for variability in annual means (Fig. 3a), with slightly higher-than-observed variability along the coast and lower-than-observed variability inland. The same spatial structure exists for inter-annual variability in DJF (Fig. 3b), MAM (Fig. 3c) and SON (Fig. 3e) seasonal means. In JJA, however, HiGEM shows considerably stronger variance than SILO across much of Queensland (Fig. 3d), although as JJA is a dry season for most of the state, small changes in the standard deviation can have a considerable effect on this statistic. For the analysis of teleconnections of seasonal Queensland rainfall to large-scale drivers (sections 4 and 5), it is promising that HiGEM shows approximately the observed levels of inter-annual rainfall variability for both seasonal and annual means. Displaying the correct levels of total inter-annual variability is necessary, but not sufficient, for producing rainfall responses of the correct magnitude to climate drivers on these temporal scales.

On decadal temporal scales, however, the variability in HiGEM rainfall displays considerably higher biases than for inter-annual scales (Fig. 4). Decadal variability is evaluated using the same ratio of normalized standard deviations as for inter-annual variability, but the time series of annual-and seasonal-mean rainfall were first smoothed using an 11 year running mean to emphasize the decadal component. HiGEM has far too little decadal variability in annual-mean rainfall across much of central Australia, including the western portions of Queensland (Fig. 4a), although the HiGEM normalised standard deviation is close to that for SILO in central and coastal Queensland. As for the inter-annual variability, the pattern of biases in DJF decadal variability (Fig. 4b) resembles that for annual mean, which is reasonable as much of Queensland rain falls in DJF., giving that season a higher weighting in annual mean. JJA rainfall in HiGEM again displays excessive variability in most of Queensland (Fig. 4d), including some regions where the annual mean was deficient, while MAM (Fig. 4c) and SON (Fig. 4e) are closer to SILO.

The results for the decadal temporal scales are less encouraging than those for the inter-annual ones, but HiGEM does produce adequate decadal variation in central and coastal Queensland. These near-observed levels of variability in HiGEM are not due to compensation errors between seasons, as all four seasons show realistic variability in these regions, except for JJA in south-eastern Queensland. Section 4.2 discusses a hypothesis for why decadal variability maybe lower than observations.

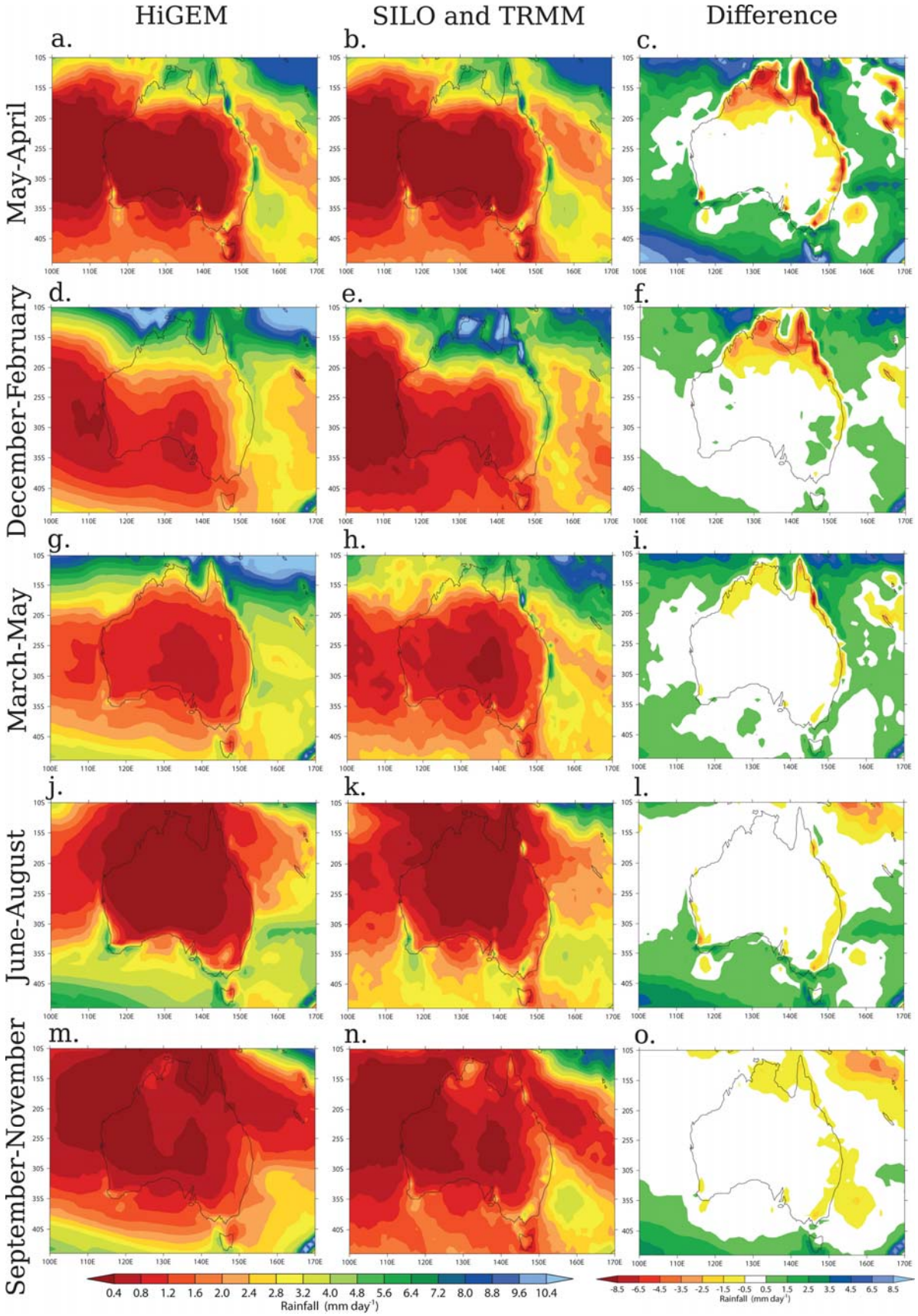

Figure 1: Climatological precipitation (mm day^{-1}) from (left) HiGEM and (centre) a combination of SILO (over land) and TRMM (over the ocean); (right) HiGEM minus the SILO/TRMM combination. The top row shows annual means; the lower four rows display seasonal means.

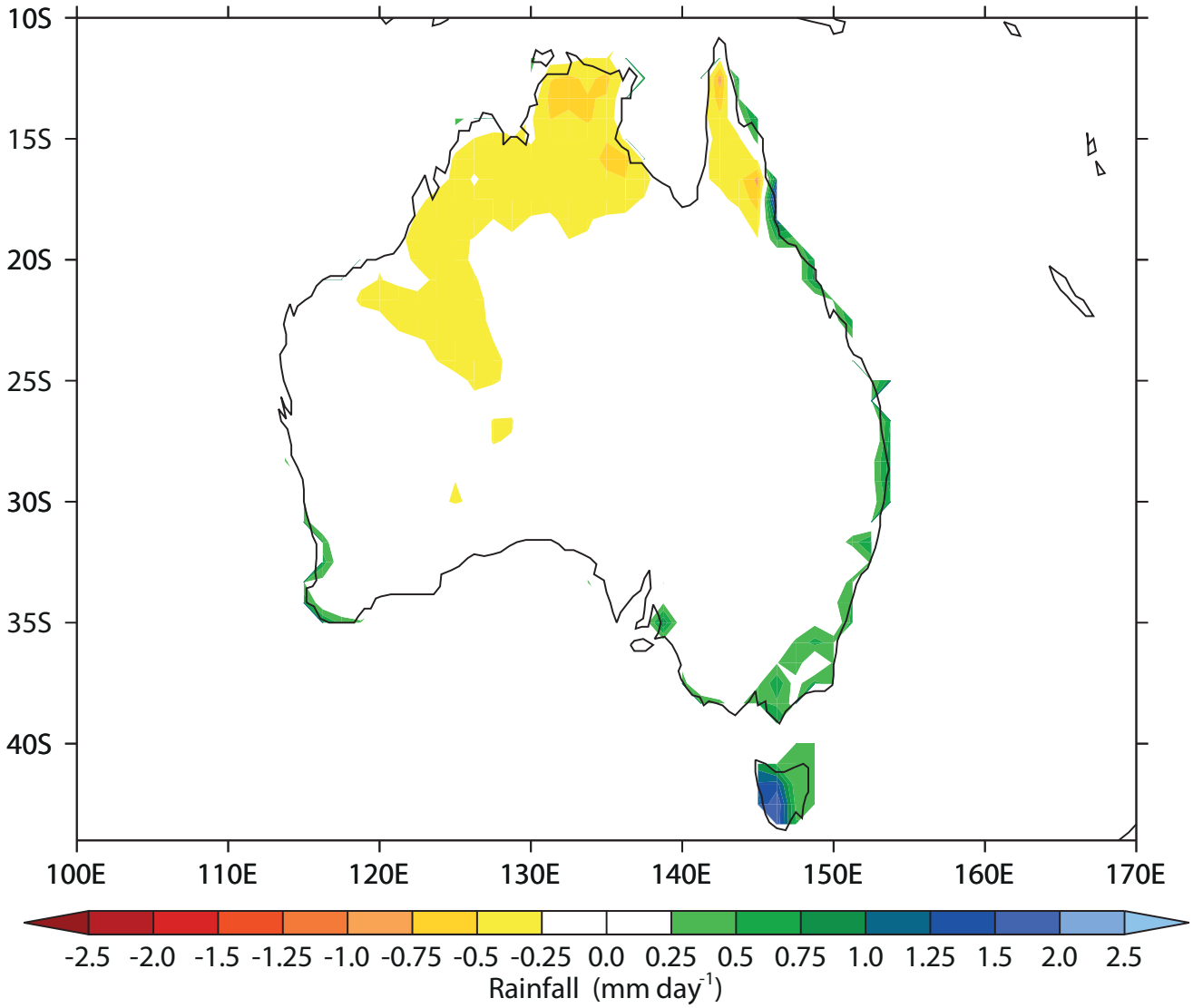

Figure 2: The difference in climatological and annual mean precipitation (mm day^{-1}) between SILO (1900-2008) and TRMM (1999-2010) over Australian land points, taken as SILO minus TRMM.

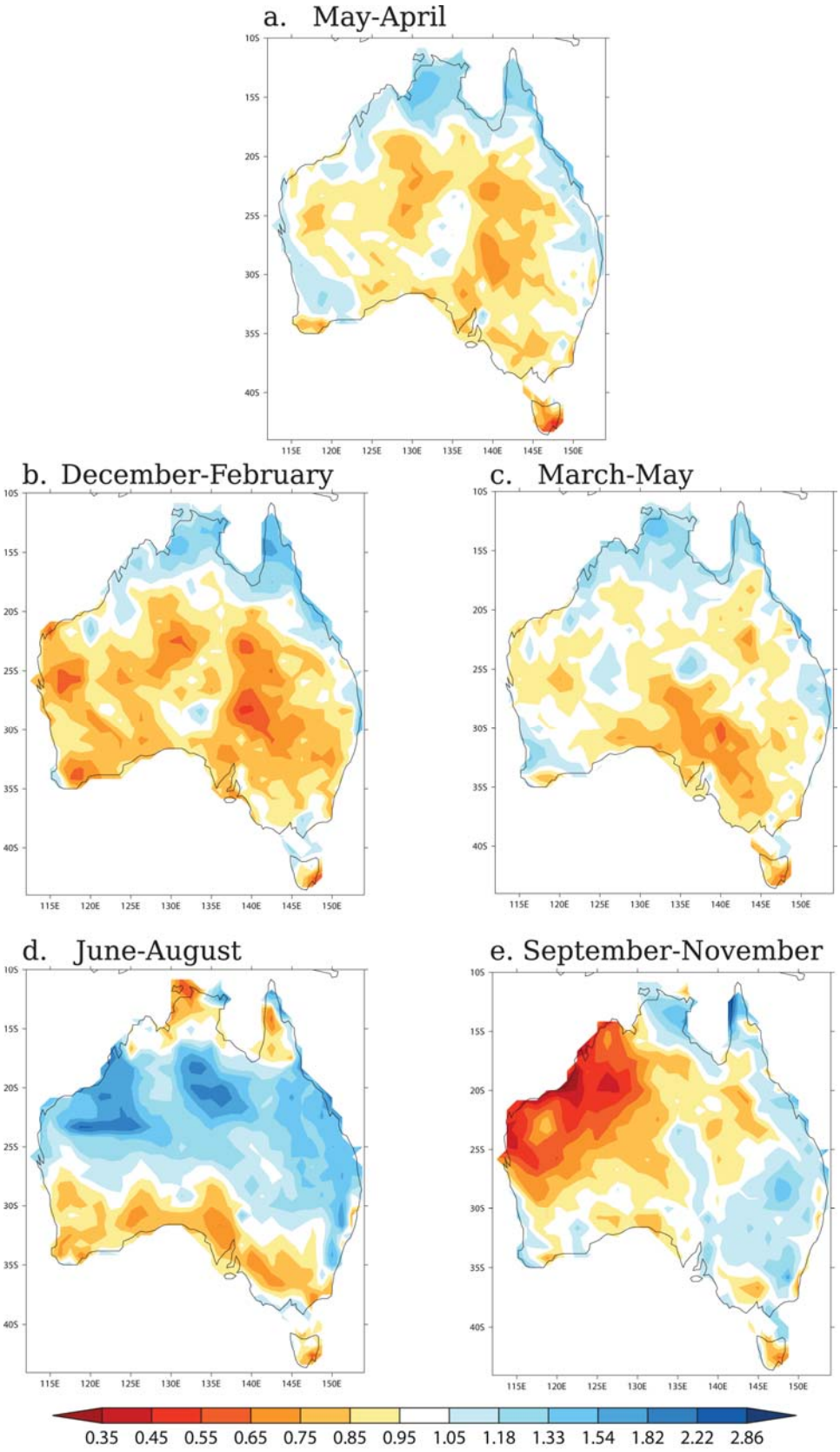

Figure 3: Ratios of normalised (by climatological precipitation) inter-annual standard deviation in precipitation (unit less) for HiGEM divided by SILO, using (a) annual-mean precipitation and (b-e) seasonal means for (b) DJF, (c) MAM, (d) JJA and (e) SON.

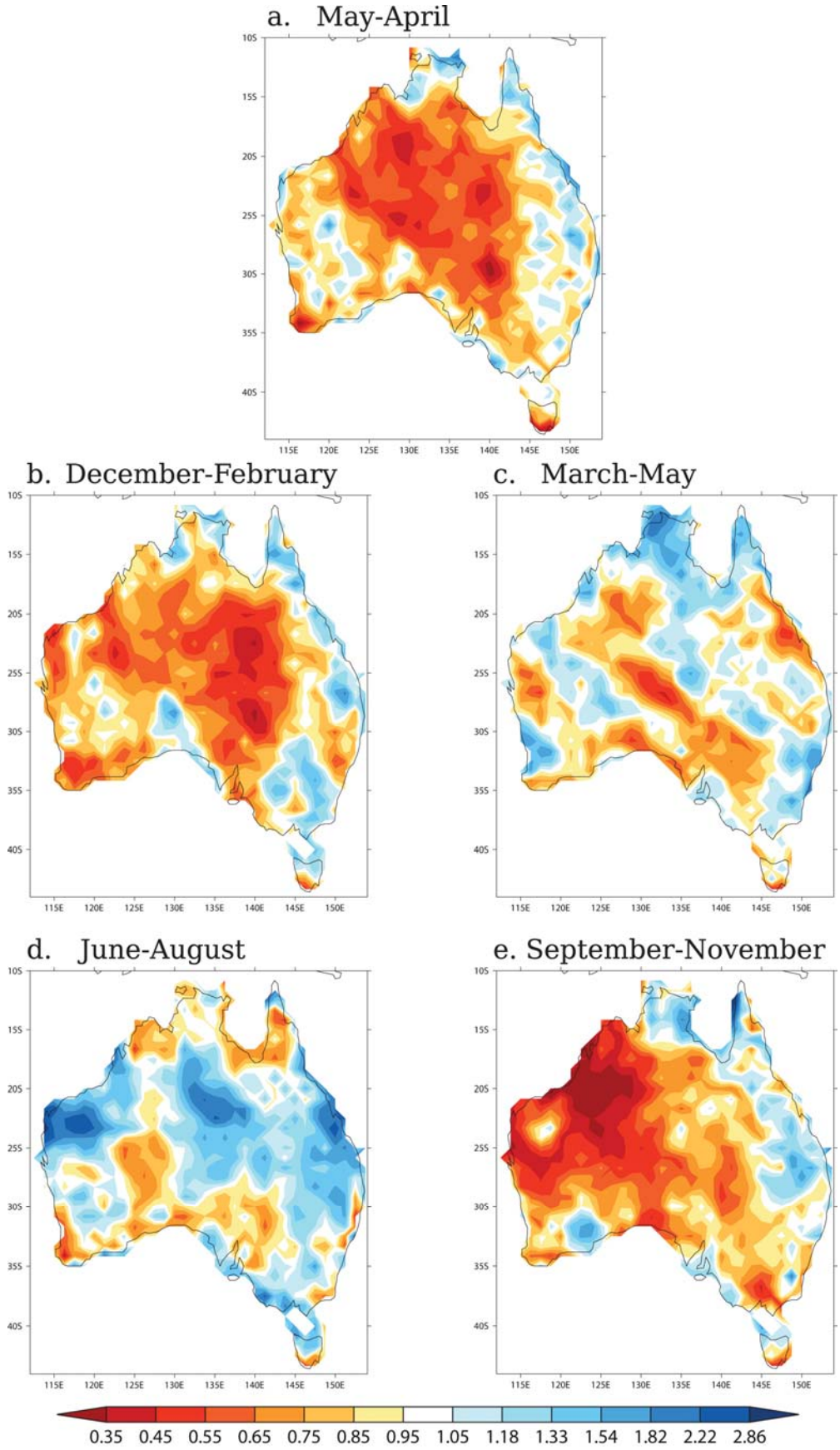

Figure 4: As in Figure 3, but using ratios of normalised inter-annual standard deviations in 11-year running-mean precipitation, to emphasize decadal variability.

5 The ability of HiGEM to simulate known drivers of Queensland rainfall variability

5.1 The El Nino–Southern Oscillation

Shaffrey et al. (2009) and Roberts et al. (2009) contain a detailed analysis of the spatial and temporal pattern of the ENSO in HiGEM, which will not be repeated here. Instead, this report focuses on the fidelity of the teleconnection in HiGEM between the ENSO and Queensland rainfall.

HiGEM successfully simulates a negative correlation of approximately the observed magnitude (from SILO and HadISST; Fig. 5a) between May–April annual-mean Niño 4 SST anomalies and May–April annual-mean rainfall across Queensland (Fig. 5b). Similar to observations (e.g., Murphy and Ribbe, 2004; Hendon et al., 2007), HiGEM produces a stronger correlation between Queensland rainfall and the central Pacific Niño 4 index than the eastern Pacific Niño 3 (not shown). The May–April annual mean is used to limit mixing phases of the ENSO in a single annual period, as the ENSO often changes sign during austral autumn. The HiGEM correlation is weaker than observed across northern Australia, which is likely due to low correlation magnitudes in HiGEM during MAM (Fig. 5h) relative to SILO/HadISST (Fig. 5d). Klingaman (2012b) found that the third MAM EOT of SILO rainfall, which described coherent rainfall variations in the Cape York Peninsula and across northern Australia, was associated with the impact of the ENSO on the strength of the late-season monsoon. The weak correlations in HiGEM in MAM may indicate that these ENSO–late-monsoon interactions are missing or suppressed in HiGEM; section 5 explores this further. In DJF (Figs. 5c and 5g), JJA (Figs. 5e and 5i) and SON (Figs. 5f and 5j), the strength and spatial pattern of the Niño 4–Queensland rainfall correlations in HiGEM closely resemble those in observations, although the HiGEM correlation is occasionally too strong. With the exception of the Cape York Peninsula, the ENSO in HiGEM explains a similar fraction of variance (approximately 30 per cent) in Queensland rainfall as the observed ENSO.

Lag correlations of area-averaged Queensland rainfall (land points in 138° –154°E, 9°–29°S) and Niño 4 SSTs reveal that while winter, spring and early summer HiGEM rainfall shows similar predictability from Niño 4 (Fig. 6b) as observations (Fig. 6a), late summer and autumn rains in HiGEM are only weakly predictable from the ENSO. In both HiGEM and SILO/HadISST, June Niño 4 SSTs are strongly correlated with rainfall from June through December, as demonstrated by the downward (i.e. longer lead time) slope of the correlation contours in June–December. In HiGEM, however, January rainfall displays an erroneously strong correlation with Niño 4 at long lead times, while the February–April lag correlations are much weaker than observed. The positive correlations in HiGEM for positive lags (i.e. rainfall leading Niño 4) in February and March are indicative of overly bi-annual ENSO variability; in other words, the ENSO in HiGEM too often switches sign in austral El Niño years. Further, the correlation for La Niña years is not affected by the outlying years, as when the four strongest La Niña events—those with May–April mean Niño 4 < -1.0°C—are removed, the correlation coefficient weakens only slightly (the dashed blue line in Fig. 7a).

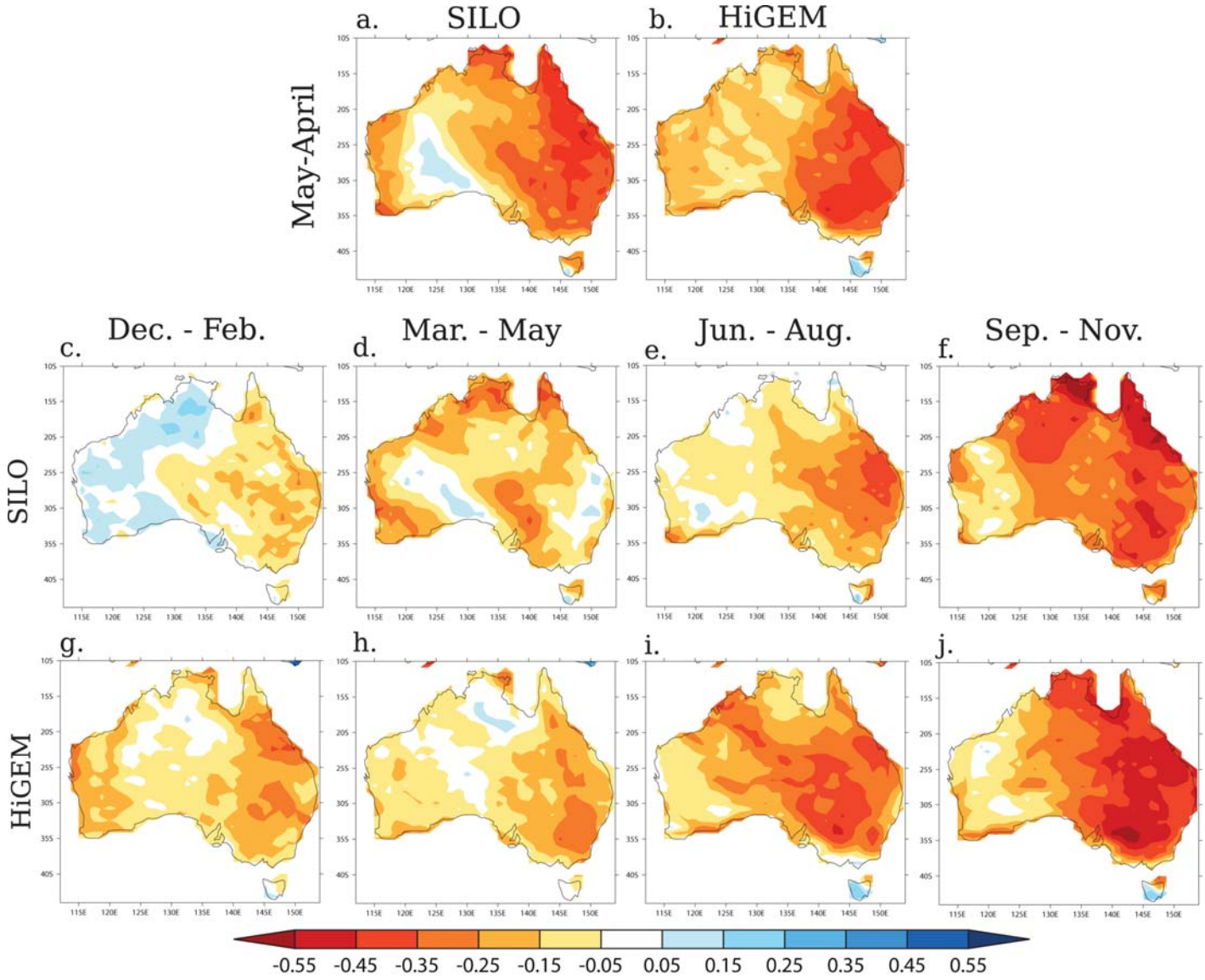

Figure 5: Instantaneous correlations between (a–b) May–April annual-mean (a) SILO rainfall and HadISST Niño 4 SSTs and (b) HiGEM rainfall and Niño 4 SSTs; (c–f) seasonal-mean SILO rainfall and HadISST Niño 4 SSTs for (c) DJF, (d) MAM (e) JJA, (f) SON; (g–j) as in (c–f) but for HiGEM rainfall and Niño 4 SSTs.

The HiGEM control integration successfully reproduces the observed asymmetric rainfall–Niño 4 relationship (Fig. 7b), with a highly significant correlation between Queensland rainfall and Niño 4 SSTs under La Niña but not under El Niño. The magnitudes of the correlations are remarkably similar to observations. The La Niña–rainfall relationship weakens somewhat when La Niña events with annual-mean SST anomalies < -1.0°C are removed (dashed blue line in Fig. 7b), more so than in observations, indicating that the agreement between HiGEM and observations is due in part to these outlying La Niña years in HiGEM. HiGEM produces quite a few strong La Niña events, three of which—those with cool anomalies stronger than -1.5°C—are stronger than any in the 1900–2008 HadISST record; the strongest two La Niñas are also the two wettest years in Queensland.

The ENSO–Queensland rainfall teleconnection is well-simulated in HiGEM, in terms of the instantaneous (Fig. 5) and lead–lag relationships (Fig. 6), the seasonal cycle of the correlation magnitude (Fig. 5) and the asymmetric response of rainfall to Niño 4 anomalies of opposite sign. There are still some minor deficiencies in HiGEM, though, including a weak rainfall–ENSO relationship in northern Queensland in autumn (Fig. 5f), an overly bi-annual ENSO period that affects the lead–lag relationships (Fig. 6b), and the fact that the La Niña– rainfall correlation is dominated by a few very strong La Niña events (Fig. 7b).

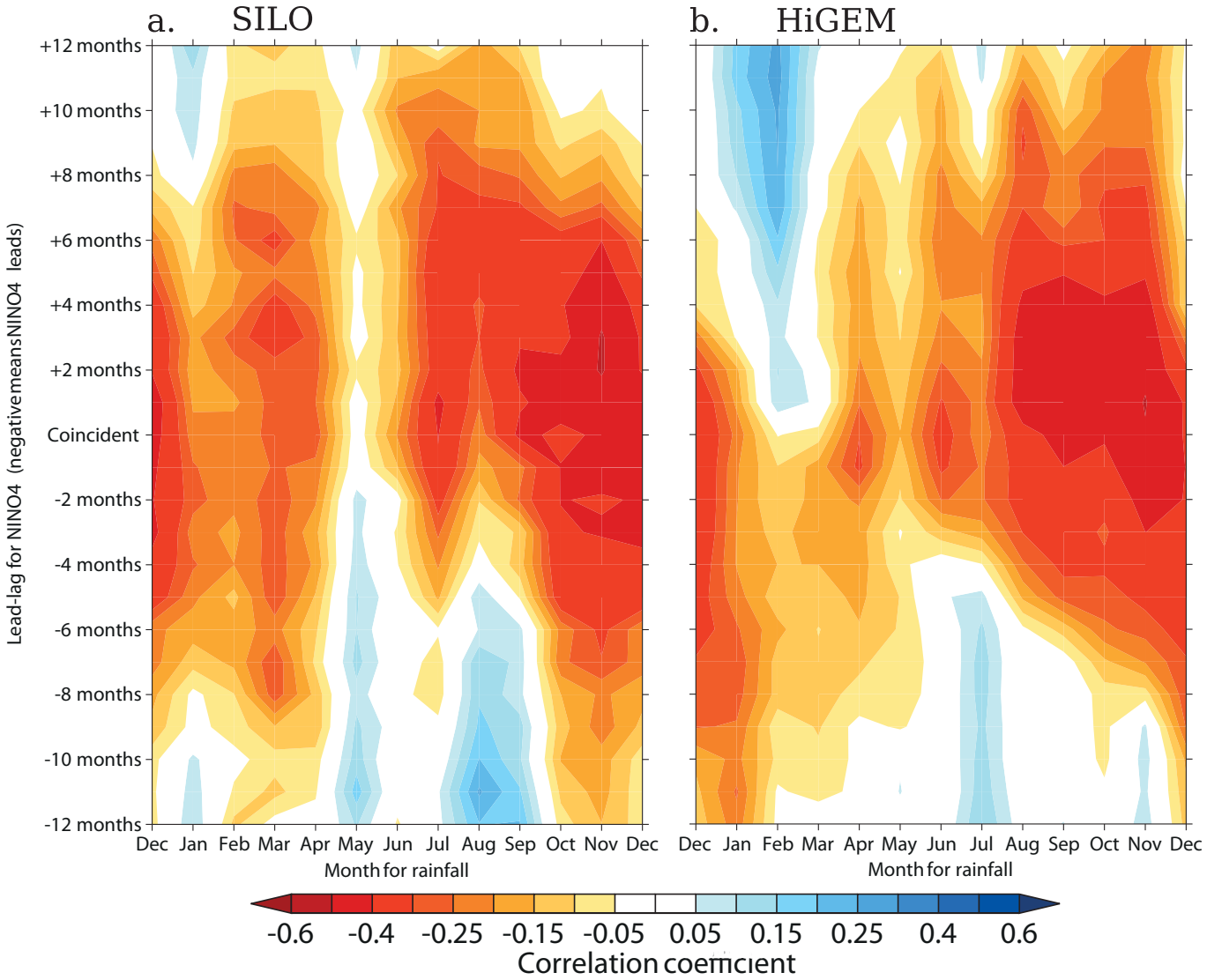

Figure 6: For (left) SILO rainfall and HadISST Niño 4 SSTs and (right) HiGEM rainfall and Niño 4 SSTs, lead–lag correlations between monthly-mean, area-averaged Queensland rainfall (138°–154°E, 9°–29°S) and monthly-mean Niño 4 SST anomalies. The horizontal axis gives the month for rainfall; the vertical axis gives the lead or lag time for Niño 4 SST anomalies, with negative (positive) values indicating that Niño 4 leads (lags) Queensland rainfall.

5.2 The Inter-decadal Pacific Oscillation

To detect the IPO in HadISST and the HiGEM and HadCM3 control integrations, the procedure of Arblaster et al. (2002) was used, itself a modified version of that of Folland et al. (1999): EOFs of 13-year lowpass filtered monthly-mean SSTs were computed for the 109 years of HadISST data, the 150 years of HiGEM output and years 101–250 of the 1000-year HadCM3 integration (Sections 2.4 and 2.5 contain further details on this method). The full 150 years of HiGEM data are used here, to give a longer record for detecting decadal variability; the first and last 13 years of each dataset are lost to the filter. The HiGEM EOFs were also computed with the first few decades removed to account for ocean spin-up, as discussed in the next paragraph.

As in Arblaster et al. (2002), the IPO is the second EOF in HadISST, as the first EOF is a uni-polar mode representing the global warming signal. The characteristic tropical–extra tropical tri-pole IPO pattern can be seen clearly in Fig. 8a. In HiGEM (Fig. 8b) and HadCM3 (Fig. 8c), EOF 1 has the highest pattern correlation with HadISST EOF 2 of any of the first ten model EOFs. While HadCM3 EOF 1 strongly resembles HadISST EOF 2, HiGEM EOF 1 shows much stronger positive loading to the east of Japan and in the North Atlantic, with reduced

magnitudes in the tropics and in the Southern Hemisphere extra-tropics. The HiGEM EOF 1 also has the wrong sign—positive instead of negative—along the west coast of North America. Thus HiGEM EOF 1 appears to be dominated by variability in the Northern Hemisphere western-boundary-current regions, rather than in the tropical and sub-tropical Pacific Ocean. This is not caused by ocean spin-up during the first few decades, as the HiGEM EOFs were re-computed with the first 20, 40 and 60 years removed: the unrealistically high variances in the western Pacific and North Atlantic remained, with little variance in the equatorial Pacific.

Using 13-year lowpass filtered SSTs, linear regressions of grid point SSTs against Niño 4 SSTs were computed for HadISST, HiGEM and HadCM3 (Figs. 8d–f). In HadISST and HadCM3, these regressions show that on decadal temporal scales, there is considerable covariation in equatorial and off-equatorial Pacific SSTs: Niño 4 SSTs are positively correlated with SSTs in the sub-tropical Pacific, the Indian Ocean and along the western coasts of North and South America, with weak negative correlations in the north-western and south-western Pacific. In HiGEM, however, Niño 4 SSTs are correlated only with themselves and some small regions in the South Pacific. This reinforces the lack of coupling between tropical and extra-tropical decadal SST variations in HiGEM, which defined the IPO in observations. Similar linear regressions of 13-year lowpass-filtered SSTs were also performed for the Niño 3, Niño 3.4 and equatorial Pacific-wide (averaged 5°S–5°Nand 150°E–90°W) regions, with similar results as for Niño 4.

Wavelet transforms of monthly-mean, unfiltered Niño 4 SSTs confirm that HiGEM lacks decadal variability in equatorial Pacific SSTs: HadISST (Fig. 8g) shows considerable decadal and multi-decadal variability in Niño 4 throughout much of the 1900–2008 period; HadCM3 (Fig.8i) has much more variability on 4–8 year periods, but does have some decadal variability; HiGEM (Fig.8h) has nearly no decadal variability that is not tied to strong inter-annual variations. The strong peak in the 3–4 year period band in HiGEM near year 110 is due to two strong La Niña events, the same two that were associated with the two wettest years in Queensland (section 4.1). Such strong variability on the 3–4 year timescale inevitably projects onto the longer, decadal temporal scale, leading to the statistically significant 10–15 year signal in HiGEM. Otherwise, there is practically no decadal variability in HiGEM Niño 4. As for the linear regressions, wavelet transforms of Niño 3, Niño 3.4 and equatorial Pacific-wide SSTs were computed, with similar results as for Niño 4. The EOFs, regressions and wavelet transforms were also performed for the other five consecutive 150 year periods of the HadCM3 control integration (i.e. years 251–400, 401–550 and so on); these periods also showed IPO-like variability that was similar to observations and much stronger than HiGEM.

Alongside limited decadal variability in rainfall (Fig. 4) over much of Australia, HiGEM lacks an IPO, as defined by coherent tropical–extra-tropical decadal variability in SSTs. On decadal temporal scales, space–time variance in SSTs is dominated by strong signals in the Northern Hemisphere boundary-current regions (Fig. 8b), with few significant correlations between equatorial and off-equatorial Pacific SSTs (Fig. 8e) and little variability in Pacific equatorial SSTs themselves (Fig. 8h).

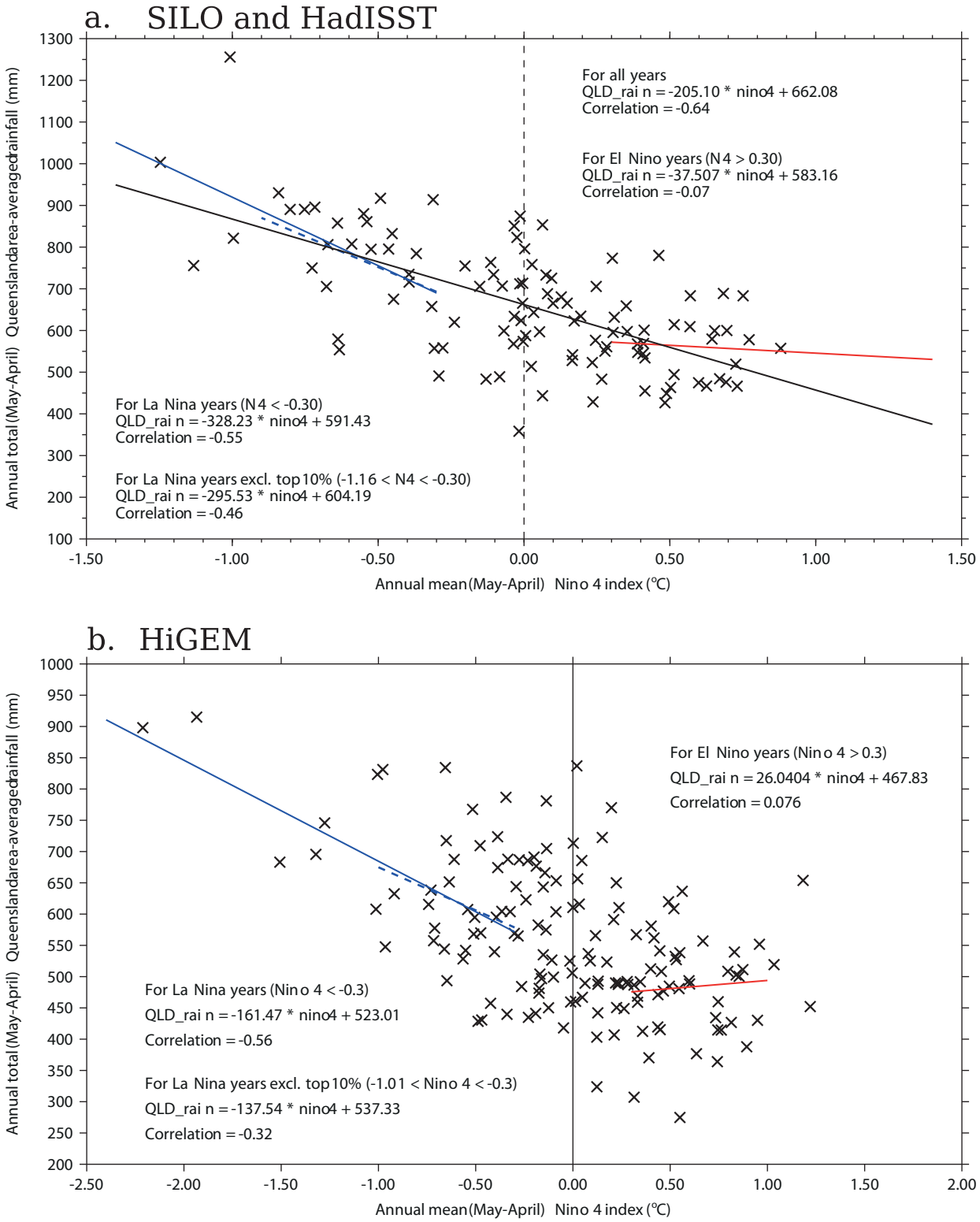

Figure 7: For (top) SILO rainfall and HadISST Niño 4 SSTs and (bottom) HiGEM rainfall and Niño 4 SSTs, scatter plots of the May–April annual mean Niño 4 SST anomalies against May–April annual-total, area-averaged (138°–154°E, 9°–29°S) Queensland rainfall. Linear-regression lines are shown for (black) all years, (solid blue) all years with a Niño 4 anomaly < -0.3°C (La Niña), (dashed line) all years with -1.0°C < Niño 4 anomaly <-0.3°C (weak or moderate La Niña), and (solid red) all years with a Niño 4 anomaly > 0.3°C.

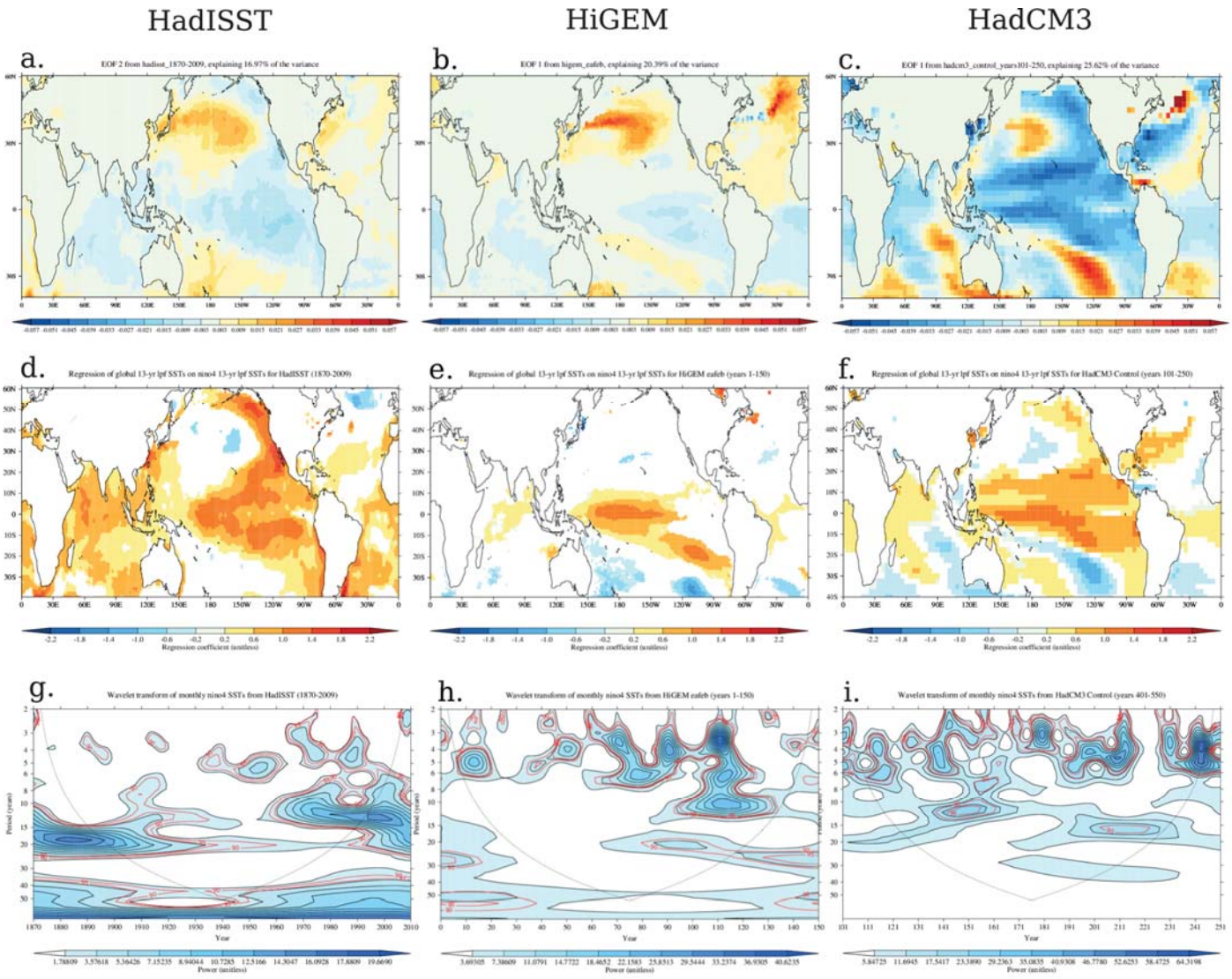

Figure 8: For (left) HadISST, (centre) the HiGEM control integration and (right) years 101–250 of the HadCM3 control integration: (top) the EOF of 13-year lowpass-filtered monthly-mean SSTs that most resembles the IPO; (middle) coefficients of linear regression of 13-year lowpass-filtered monthly-mean SSTs onto 13-year lowpass filtered monthly-mean Niño 4; (bottom) the wavelet transform of monthly-mean Niño 4 SSTs, using a Morlet mother wavelet, with the 90 per cent and 95 per cent confidence levels marked in red contours. Regression coefficients are shown only where correlations are statistically significant at the 5 per cent level. The dotted line in the wavelet diagrams shows the "cone of influence", outside of which edge effects dominate the signal and the results are not robust.

5.3 Tropical Cyclones

In its climatology, HiGEM produces more tropical cyclones tracks near the northern Australian coast (Fig. 9a) than observed (Fig. 9b), particularly west of the Gulf of Carpentaria. Near Queensland the HiGEM track densities resemble observations, although they are likely too many storms near the Cape York Peninsular and too few along the eastern coast further south (Fig. 9c). The long "tail" of HiGEM tracks extending southeast, past New Zealand, are due to continued tracking of cyclones after they become extra-tropical; these transitions are not included in observations (section 2.6). Still, HiGEM track densities are far too large east of the dateline.

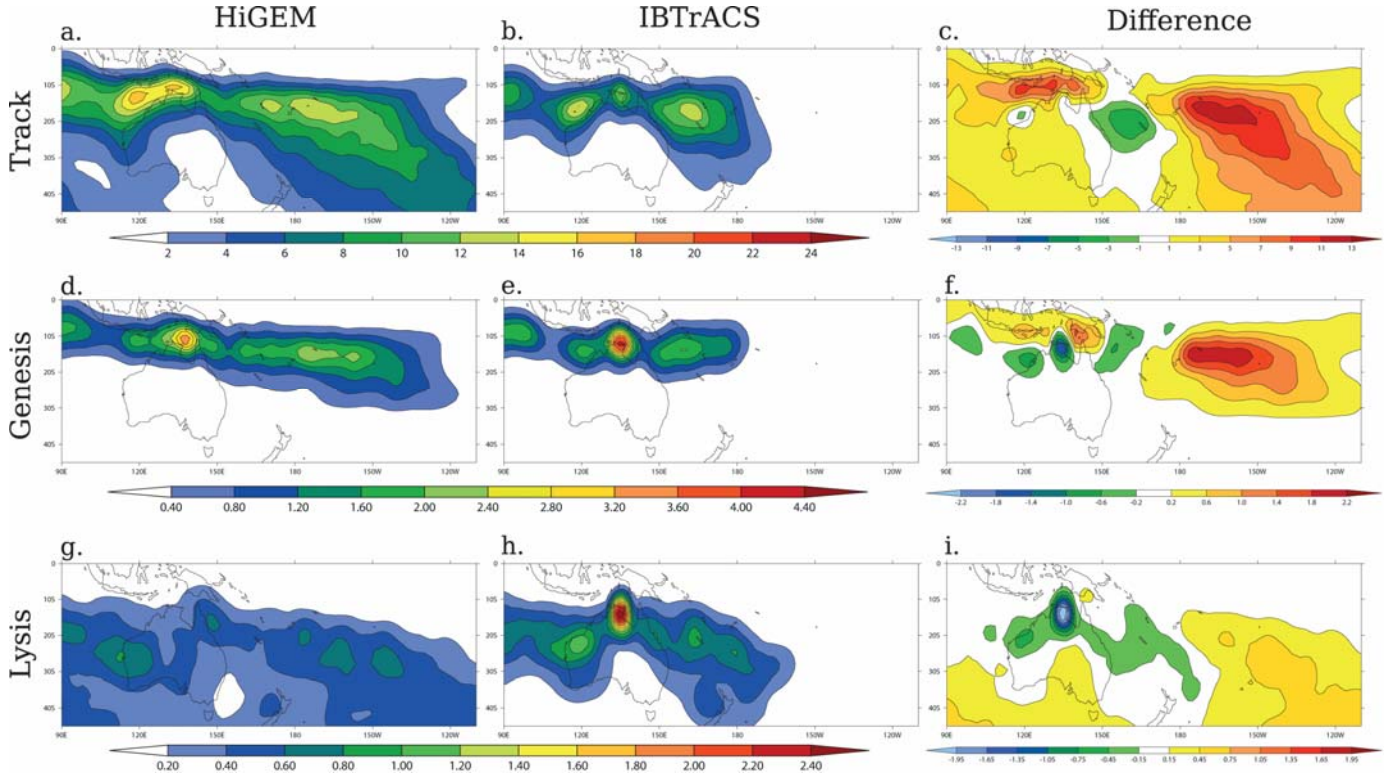

Figure 9: For (left) IBTrACS observations and (middle) HiGEM and (right) HiGEM minus IBTrACS: climatological October–May-mean (top) track density, (middle) genesis density and (bottom) lysis density of tropical cyclones. Densities are in units of cyclones season^{-1} within a 5° spherical cap of each T62 (approximately 1.9° × 1.9°) grid point. The unit area is approximately equal to 10^6 km^2; see section 2.6 for further details.

Most cyclones in HiGEM are generated just south of the Gulf of Carpentaria (Fig. 9d). The peak there is remarkably similar to the observed peak in genesis density (Fig. 9e). Genesis densities in the Coral Sea are also similar to IBTrACS (Fig. 9f), although, as seen in the track densities, HiGEM forms far too many tropical cyclones east of the dateline.

Many observed cyclones "die" near Darwin, with secondary maxima along the western and eastern coasts (Fig. 9h). HiGEM produces these secondary maxima well, but fails to simulate the maximum near Darwin (Fig. 9g). This is likely due to different treatment of extra-tropical transitions in IBTrACS and HiGEM; the fact that extra-tropical cyclones continue to be tracked in HiGEM leads to a wider variety of lysis locations that are generally further south than in observations (Fig. 9i).

While tropical cyclones are considered as potential drivers of rainfall EOTs in Section 5 - as they were in Klingaman (2012b) for observations - this report does not consider the inter-annual or decadal variability of tropical cyclones in HiGEM, or the connections in variability of those temporal scales to large-scale drivers (e.g. the ENSO).

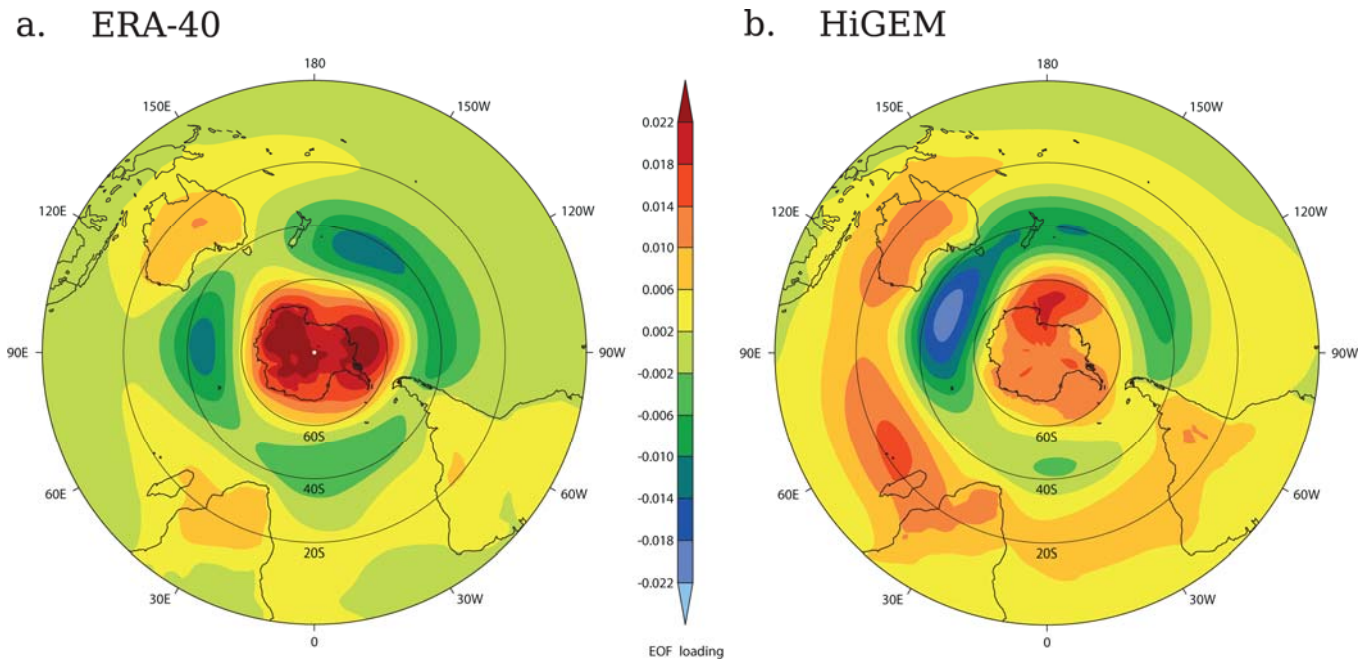

Figure 10: The spatial structure of the leading EOF of monthly-mean, Southern Hemisphere surface pressures in (left) ERA-40 and (right) HiGEM.

5.4 The Southern Annular Mode

The SAM frequently emerges as the first EOF of the southern hemispheric surface pressure in GCMs, observations and reanalysis data (e.g. Thompson and Wallace, 2000). Here, we compare the first EOFs of monthly-mean, Southern Hemispheric surface pressures in the 1958-2002 European Centre for Medium Range Weather Forecasting reanalysis (ERA-40; Uppala et al. 2005, Fig. 10a) and HiGEM (Fig. 10b). The HiGEM EOF broadly resembles that from ERA-40, but HiGEM has reduced variability over Antarctica - with the positive pole there shifted away from the South Pole - and increased variability in the Southern Ocean south of Australia. The SAM in HiGEM also has pronounced tri-pole pattern than in observations, with a stronger third, positive pole near 20°S. HiGEM EOF 1 explains 27.2 per cent of the total space-time variance in HiGEM Southern Hemisphere total pressure, similar to ERA-40 EOF 1, which explains 24.1 per cent of the ERA-40 variance.

The connection between HiGEM SAM and rainfall in Queensland is explained in Section 5, when the SAM is investigated as a potential driver for EOTs of HiGEM seasonal rainfall.

6 EOT analysis of Queensland rainfall in HiGEM

In this section, the leading four EOTs of HiGEM seasonal Queensland rainfall are introduced (Section 5.1) then compared to the leading three EOTs of SILO seasonal rainfall, as discussed in Section 2.7. Appendix A reproduces the spatial patterns (Fig. 24) and time series (Fig. 25) of the SILO EOTs, as well as the tables giving the correlations with proposed large-scale modes (Table 3) and the mechanisms that Klingaman (2012b) concluded drove each EOT (Table 4).

6.1 Spatial and temporal patterns

As for the SILO EOTs in Klingaman (2012b), the leading seasonal HiGEM EOTs display a uni-polar spatial pattern, indicating that they describe coherent variations in rainfall across much of Queensland (Figs. 11a–d). EOT 1 for DJF (Fig. 11a) and MAM (Fig. 11b) are concentrated in the north, as in SILO (Figs. 24a and 24b). The central point in the HiGEM MAM EOT 1, however, is located much further north and west than in the corresponding SILO EOT, with lower correlations in south-eastern Queensland. JJA EOT 1 in HiGEM (Fig. 11c) is nearly identical to that from SILO (Fig. 24c), while SON EOT 1 (Fig. 11d) is shifted south relative to SILO (Fig. 24d) with weak correlations in north-eastern Queensland. These spatial shifts suggest a more abrupt seasonal transition in HiGEM between the summer rainfall regimes—when the rain is heaviest in the north of Queensland—and the winter regime—when the south of the state receives more rain than the north.

Once the leading EOTs have been removed, the remaining HiGEM EOTs describe coherent regional variations in seasonal rainfall. The spatial patterns of HiGEM EOTs 2–4 generally show less agreement with those from SILO. Even slight differences in the spatial patterns of the first EOTs can cause considerable changes in the remaining EOTs, since each EOT depends upon the ones preceding it. These differences become compounded in EOTs beyond the second, as EOT 3, for example, depends on the first two EOTs. Also, EOTs beyond the first explain similar percentages of the total variance in both HiGEM (Table 1) and SILO (Table 3). Small variations in these percentages between HiGEM and SILO, then, could lead to differences in the order of the EOTs, which again would affect the lower-order patterns as each EOT depends upon the ones preceding it. For these reasons, the first six EOTs from HiGEM were computed to compare with the three leading SILO EOTs, although none of the HiGEM EOTs 5 or 6 were similar to any of the SILO EOTs 1–3 (section 2.7). Still, there are some notable similarities between the regional HiGEM and SILO EOTs, including HiGEM DJF EOT 4 (Fig. 11i) and SILO DJF EOT 2 (Fig. 24e), HiGEM JJA EOTs 2 and 3 (Figs. 11g and 11k) and their SILO counterparts (Figs. 24g and 24k) and HiGEM SON EOT 4 (Fig. 11p) and SILO SON EOT 3 (Fig. 24l). The following sub-sections will evaluate whether the HiGEM EOTs are driven by the same mechanisms as those from SILO.

Time series of each HiGEM EOT are shown in Figure 12. As for the SILO EOTs (Fig. 25), there are practically no statistically significant 31-year running linear trends in the HiGEM EOTs, shown by the scarcity of red dots along the horizontal axes of Figure 12. While SILO DJF EOT 1 demonstrated considerable decadal and multi-decadal variability, which Klingaman (2012b) showed was associated with the IPO (see Fig. 5a in that report), the wavelet transform of HiGEM DJF EOT 1 displays only limited 8–10 year variability for a portion of the simulation (Fig. 13a). This is consistent with the lack of both decadal variability in Queensland rainfall (section 3) and an IPO (section 4.2) in HiGEM. Several other, regional HiGEM rainfall EOTs do show some decadal and multi-decadal variability, however, particularly JJA EOT 2 and SON EOT 4 (Figs. 13d and 13e, respectively); DJF EOT 2 and MAM EOT 2 also have limited power on these temporal scales (Figs. 13b and 13c, respectively). Of these, the spatial patterns of HiGEM DJF EOT 2, MAM EOT 2 and JJA EOT 2 resemble SILO DJF EOT 3, MAM EOT 2 and JJA EOT 2, respectively; these SILO EOTs also demonstrated decadal or multidecadal variability in Klingaman (2012b) (see Fig. 5 in that report) which was shown to be driven by internal variations in local synoptic circulation patterns (e.g. onshore winds). Section 5.2.4 analyses whether the corresponding HiGEM EOTs are driven by similar mechanisms. While the spatial pattern of HiGEM SON EOT 4 (Fig. 11p) is similar to SILO SON EOT 3 (Fig. 24l), the SILO EOT did not display any decadal or multi-decadal variability.

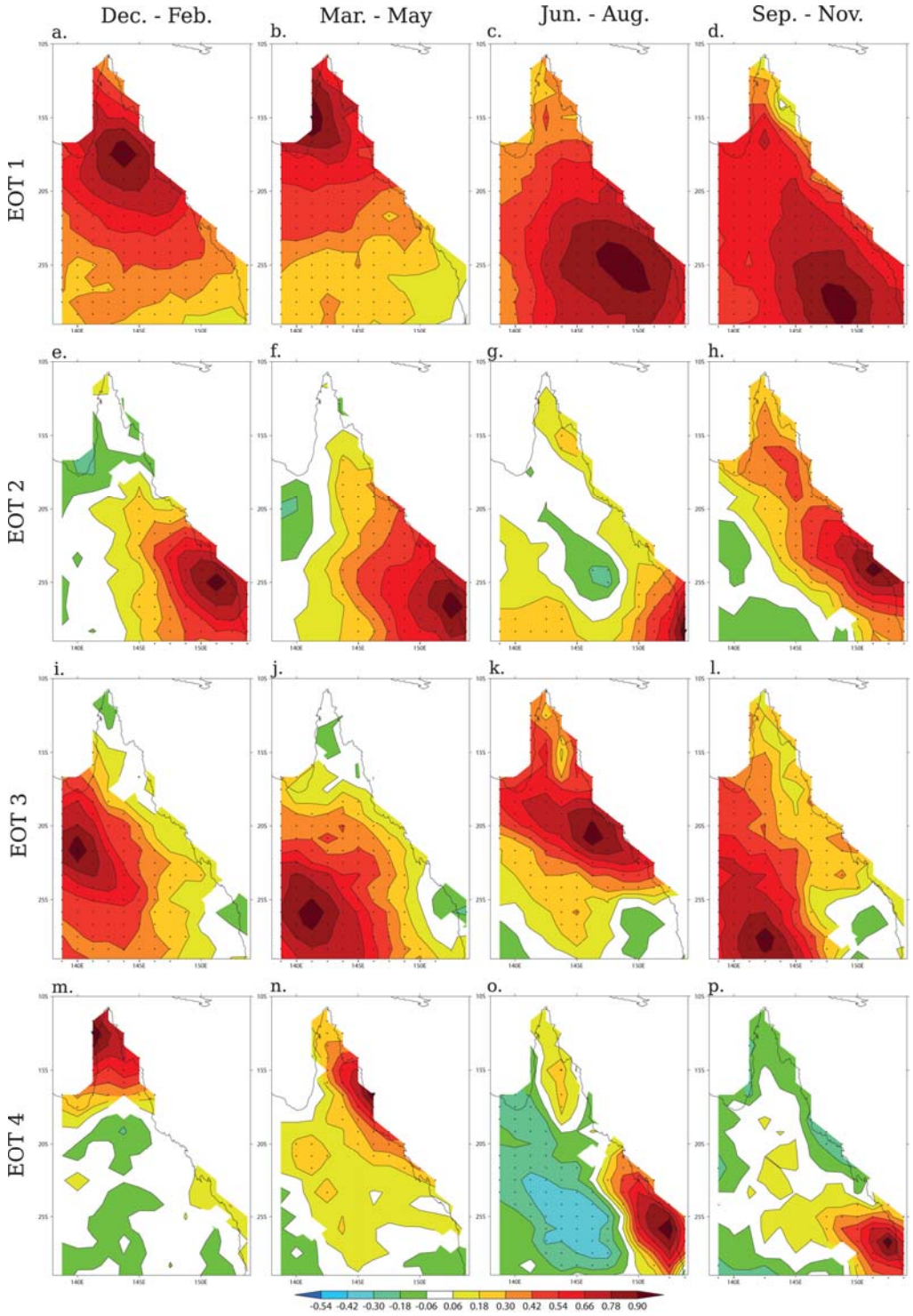

Figure 11: Spatial patterns of the first four empirical orthogonal teleconnections (EOTs) of seasonal HiGEM Queensland rainfall, using years 21–150 of the control integration, computed as the correlations of each grid point with the central grid point for each EOT (marked with a black triangle). Stippling indicates statistically significant correlations at the 5 per cent level.

6.2 HiGEM EOTs with SILO counterparts

In this section, those HiGEM EOTs with clear SILO counterparts—both in the region affected and in the mechanism producing rainfall variations—are analysed. As in Klingaman (2012b), the discussion of the EOTs is

divided by mechanism: the ENSO (Section 5.2.1), tropical cyclones (Section 5.2.2), the continental-scale monsoon circulation (Section 5.2.3) and local synoptic circulations (Section 5.2.4). Section 5.3 discusses those HiGEM EOTs 1–3 that do not match those from SILO. As four HiGEM EOTs are compared against only three from SILO, there will clearly be one additional, non-matching HiGEM EOT in each season. The non-matching HiGEM EOT in each season that explains the least variance is analysed briefly in Section 5.4 as an "additional EOT"; in MAM, JJA and SON this is EOT 4, while in DJF it is EOT 3. Table 2 shows, for each HiGEM EOT, the percentage of variance explained, the region affected, the driving mechanism and the matching SILO EOT, if any.A similar table for SILO can be found in Appendix A as Table 4.

The relevant regressions (e.g. on SSTs, 850 hPa winds, mean-sea-level pressure) from HiGEM on each EOT will be shown alongside those from observations and reanalysis. The latter regressions are reproduced from Klingaman (2012) for convenience; the data sources are not repeated here, however. For consistency, the figure captions refer to all regressions onto EOTs computed from SILO rainfall analyses as “SILO EOTs”, instead of using the name of the observed dataset or reanalysis (e.g. HadISST for SSTs, the 20th Century Reanalysis (20CR) for atmospheric circulation fields).

6.2.1 ENSO-driven patterns

The leading, state-wide HiGEM rainfall EOTs in DJF, JJA and SON show statistically significant correlations with Niño 4 (Table 1), as for SILO (Table 3). HiGEM produces equatorial Pacific SST anomalies in association with DJF EOT 1 that resemble ENSO (Fig. 14a), but these are meridionally confined and extend too far west compared to the regression of HadISST SSTs on SILO DJF EOT 1 (Fig. 14d). HiGEM also lacks the extra-tropical Pacific SST anomalies in each hemisphere found in HadISST, which Klingaman (2012b) determined were the signature of the IPO; SILO DJF EOT 1 is strongly correlated with the IPO (Table 3). This further suggests the lack of an IPO in HiGEM. The DJF EOT 1 low-level circulation pattern in HiGEM (Fig. 14g) broadly agrees with that from the 20CR for the SILO EOT (Fig. 14j), with an enhanced monsoon cyclone over continental Australia. The cyclone is shifted too far east in HiGEM, however, and there is no sign of the positive pole of the Southern Oscillation, which appears in 20CR. The region of anomalous equatorial convergence in HiGEM is centred over the Maritime Continent, further west than in 20CR, which is consistent with a westward displacement of the anomalous Walker Circulation in HiGEM due to the extension of the ENSO-driven SST anomalies into the West Pacific. The combination of the displacements to the anomalous Walker Circulation and monsoon anticyclone in HiGEM produces an erroneous anomalous anti-cyclonic circulation in the Coral Sea northeast of Australia.

The HiGEM SST patterns associated with JJA EOT 1 (Fig. 14b) and SON EOT 1 (Fig. 14c) are in closer agreement with observations (Figs. 14e and 14f, respectively) than those for DJF EOT 1. In each season, though, the maximum HiGEM SST variability occurs in the central Pacific—close to the Niño 4 region—whereas the HadISST observations show equal amounts of variability in the central and eastern Pacific.

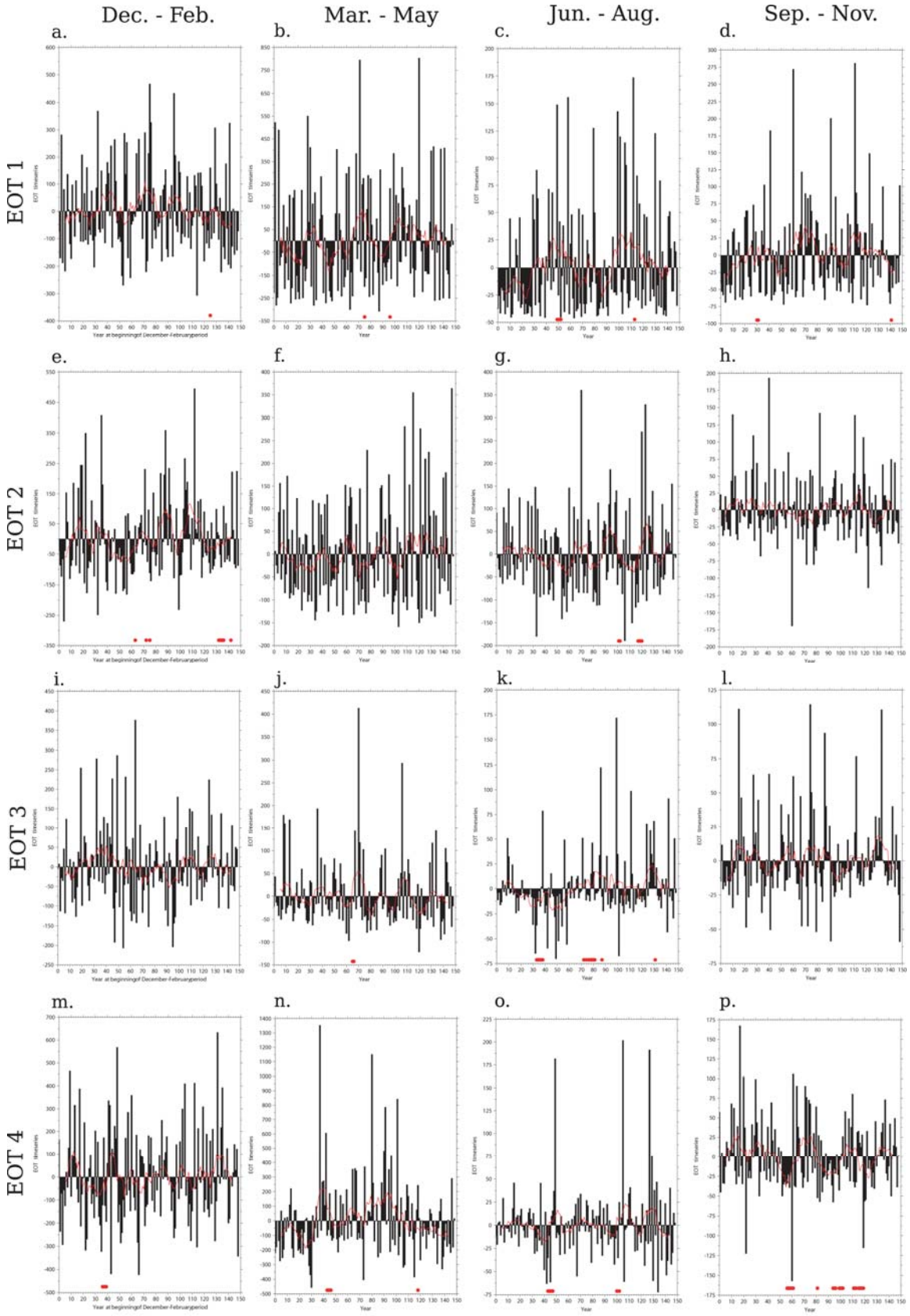

Figure 12: Time series of each of the four leading EOTs of seasonal HiGEM Queensland rainfall, arranged as for the spatial patterns in Fig. 11. The time series are expressed as anomalies from their mean, to aid interpretation. Red dots along the horizontal axis indicate where the 31-year running linear trend, computed using the 15 years before and after the dot, is statistically significant at the 5 per cent level.

Season and EOT	Variance explained	Niño 4	$B_{120\ 150}$	$B_{150\ 180}$	SAM	$SAM_{Niño\ 4}$	IOD	$IOD|_{Niño\ 4}$
December–February								
EOT 1	32.18%	-0.28**	0.21*	0.23*	0.10	0.09	-0.18*	-0.08
EOT 2	9.80%	-0.15	0.27**	0.18*	0.16	0.14	-0.10	0.01
EOT 3	7.86%	-0.03	-0.08	-0.03	-0.05	-0.05	-0.05	-0.04
EOT 4	7.10%	-0.02	-0.06	-0.04	0.06	0.06	0.04	0.06
March–May								
EOT 1	28.59%	-0.10	-0.21*	-0.10	0.08	0.08	0.06	0.06
EOT 2	14.55%	-0.14	0.24**	0.13	0.16	0.15	0.08	0.08
EOT 3	7.10%	-0.25*	0.20*	0.03	0.11	0.10	-0.01	-0.01
EOT 4	7.00%	-0.14	0.01	-0.05	0.02	0.01	0.09	0.09
June–August								
EOT 1	46.56%	-0.37**	0.23*	-0.00	0.11	0.07	-0.27**	-0.15
EOT 2	16.39%	0.04	0.29**	0.25**	0.27**	0.28**	0.14	0.14
EOT 3	6.90%	-0.09	-0.11	-0.09	0.07	0.06	-0.25**	-0.23**
EOT 4	4.23%	-0.05	-0.00	-0.09	0.00	-0.00	0.13	0.16
September–November								
EOT 1	48.60%	-0.53**	0.40**	0.17	0.42**	0.36**	-0.38**	-0.10
EOT 2	9.89%	-0.15	0.11	0.21*	0.15	0.12	-0.13	-0.05
EOT 3	7.75%	-0.24**	0.09	0.26**	0.08	0.13	-0.18*	-0.05
EOT 4	4.00%	-0.07	-0.07	-0.14	0.11	0.09	-0.05	-0.01

Table 1: For the leading four HiGEM EOTs of seasonal rainfall: the percentage of variance in the area-averaged Queensland rainfall that the EOT explains; instantaneous correlation coefficients between each EOT and Niño 4 SSTs, the Bureau of Meteorology blocking index longitude averaged over 120°–150°E (B120–150) and 150°E–180° (B120–150), the Marshall (2003) index of the Southern Annular Mode (SAM) and the Saji et al. (1999) index of the Indian Ocean Dipole (IOD). For the SAM and the IOD, the partial correlations with Niño 4 SSTs are also computed ($SAM|_{Niño\ 4}$ and $IOD|_{Niño\ 4}$, respectively). A * (**) indicates the correlation is statistically significant at the 5 per cent (1 per cent) level.

HiGEM correctly generates warm SST anomalies near Australia and the Maritime Continent during high JJA and SON EOT 1 years, consistent with La Niña in the central Pacific. There are strong suggestions of negative IOD events during wet springs in both HiGEM and observations, although the correlation with the IOD is statistically significant only in HiGEM (compare SON EOT 1 in Tables 1 and 3). Neither HiGEM nor HadISST produce a statistically significant partial correlation between the IOD and SON EOT 1, however, once the effects of Niño 4 have been removed from each. This suggests that the IOD and ENSO co-vary in HiGEM and in observations; past studies have concluded that the IOD does not influence eastern Australian rainfall independently from ENSO (e.g. Nicholls 1989; Murphy and Ribbe 2004; Risbey et al. 2009).

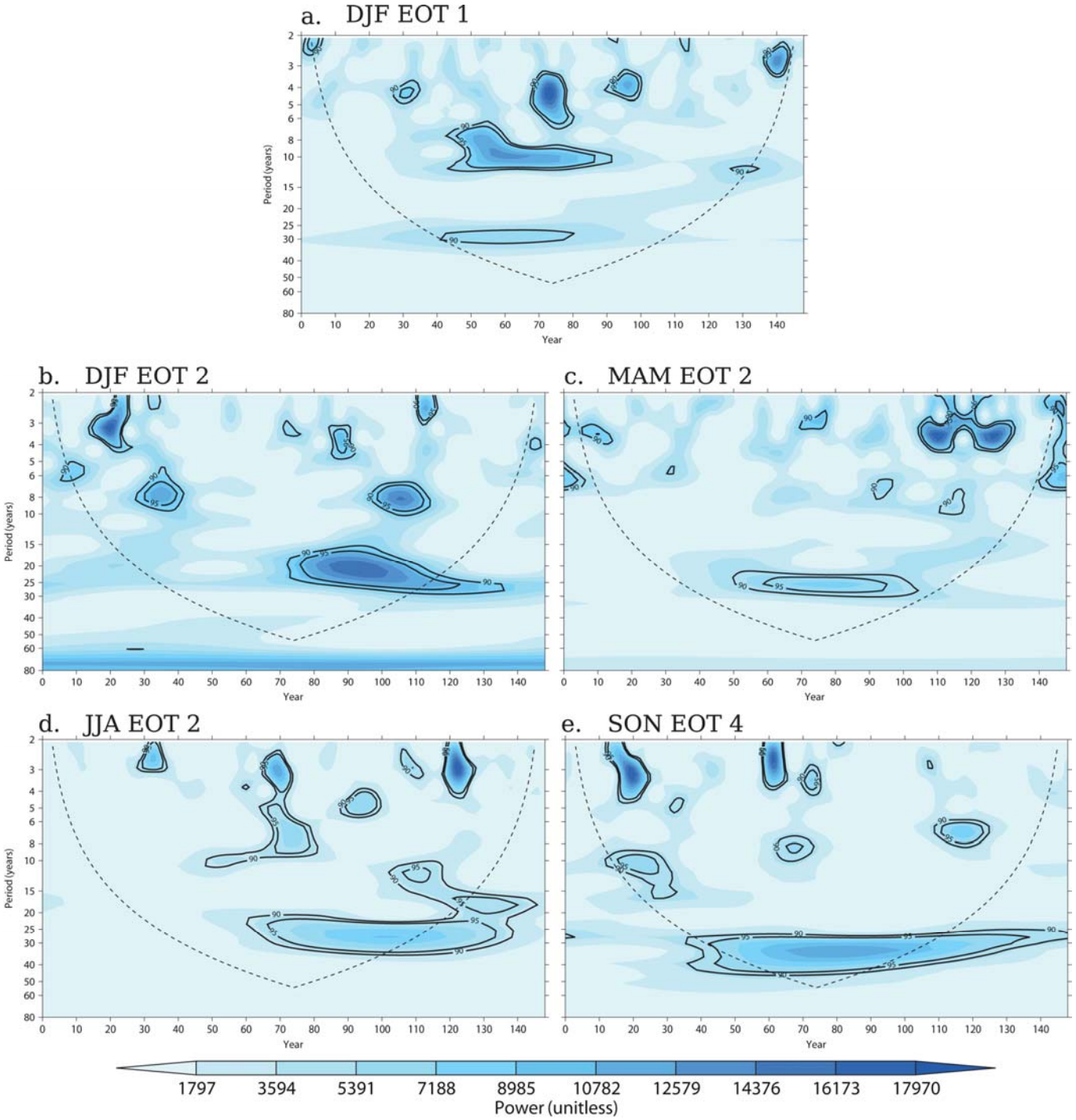

Figure 13: Wavelet transforms of selected HiGEM EOTs, using a Morlet mother wavelet. The 90 per cent and 95 per cent confidence intervals are drawn in thick solid contours and labelled. The dashed contour represents the cone of influence, outside of which the edge effects of the wavelet filtering technique dominate and the results cannot be trusted.

State-wide Queensland rainfall in winter and spring is associated with tropical and extra-tropical lower tropospheric circulation anomalies in HiGEM (Figs. 14h and 14i), as in 20CR (Figs. 14k and 14l). Klingaman (2012b) hypothesised that the extra-tropical circulation anomalies, which in observations were correlated with the SAM, could be explained only as the combined effects of the ENSO and the SAM as the partial correlations between the SAM and the EOT 1 patterns, removing the influence of Niño 4 on both, was statistically significant (Table 3). HiGEM produces a strong correlation with the SAM in spring (Table 1), which in observations remains significant when the partial correlation with Niño 4 is computed, but there is no significant correlation in winter. State-wide

JJA rainfall in HiGEM is therefore related to only the ENSO-driven tropical circulation. The relationships between these EOTs and the SAM will be examined further in Section 5.2.5. The 850 hPa circulations over Queensland in HiGEM (Figs. 14h–i) are remarkably similar to those from 20CR (Figs. 14j–k), with enhanced cyclonic circulation over northern Australia and anomalous onshore winds along the Queensland coast in both winter and spring. The strong blocking anti-cyclone over New Zealand during wet SON seasons in Queensland is also reproduced well in HiGEM.

Season and EOT	Variance explained	Region affected	Likely driving mechanism	Matching SILO EOT
December–February				
EOT 1	32.18%	State-wide	ENSO (peaking) effects on Australian monsoon	DJF EOT 1
EOT 2	9.80%	Southern	Coastal cyclonic activity and moisture transport	DJF EOT 3
EOT 3	7.86%	Northwestern	Enhanced local monsoon circulation and moisture transport	None
EOT 4	7.10%	Cape York	Tropical cyclone activity in the Coral Sea	DJF EOT 2
March–May				
EOT 1	28.59%	State-wide	Late-season monsoon circulation, but weaker than observed	MAM EOT 1
EOT 2	14.55%	Central and southern	Coastal cyclonic activity	MAM EOT 2
EOT 3	7.10%	Western	Weak ENSO (decaying) relationship	None
EOT 4	7.00%	Northern coastal	Tropical cyclone activity in the Coral Sea	None
June–August				
EOT 1	46.56%	State-wide	ENSO (developing) and onshore winds	JJA EOT 1
EOT 2	16.39%	Southeastern	Blocking in Southern Ocean and onshore winds	JJA EOT 2
EOT 3	6.90%	Northern	Southward moisture advection across Cape York	None
EOT 4	4.23%	Southeastern and western	Unknown, no significant regressions	None
September–November				
EOT 1	48.60%	State-wide	ENSO (developing), Southern Ocean blocking and the SAM	SON EOT 1
EOT 2	9.89%	Coastal and northern	Moist air and low pressures offshore	None
EOT 3	7.75%	Western	ENSO (decaying)	None
EOT 4	4.00%	Southeastern	Unknown, no significant regressions	None

Table 2: For each HiGEM EOT of seasonal rainfall, the percentage of variance in the all-Queensland rainfall that the EOT explains, the region of Queensland most affected by the EOT, the mechanism likely responsible for driving the EOT, and whether the EOT matches one of the leading three EOTs from SILO, both in terms of its spatial location and its driving mechanism.

Lag regressions of monthly-mean Niño 4 SSTs are used to evaluate whether HiGEM shows the same temporal evolution of Niño 4 SSTs associated with each ENSO-driven EOT as in observations (Fig. 15). For the leading summer and winter EOTs (Figs. 15a and 15c), HiGEM shows considerably lower regression coefficients than observations (Figs. 15b and 15d); HiGEM also lacks the observed peak in Niño 4 SST anomalies in DJF. Further examination reveals that this is due to a low standard deviation in Niño 4 SSTs in HiGEM, not to a low correlation coefficient (not shown). Regressions on HiGEM DJF EOT 1 show erroneous positive correlations in the following austral spring, which provides further evidence of the overly bi-annual ENSO variability in HiGEM identified in the lead–lag correlations of Niño 4 and Queensland rainfall (Fig. 6b). Only SON EOT 1 in HiGEM is related to strengthening Niño 4 SSTs that peak in the following DJF, as in HadISST.

There are two additional HiGEM EOTs—MAM EOT 3 and SON EOT 3—that show statistically significant correlations with Niño 4. While SILO also has one EOT in MAM (MAM EOT 3) and a second EOT in SON (SON EOT 2) that are driven by ENSO (Table 4), these HiGEM EOTs influence different regions of Queensland than the SILO EOTs: HiGEM MAM EOT 3 and SON EOT 3 describe rainfall variability in southwestern Queensland, while SILO MAM EOT 3 and SON EOT 2 are restricted to the tropical north. As these HiGEM EOTs do not agree with SILO, they are discussed in Section 5.3.1.

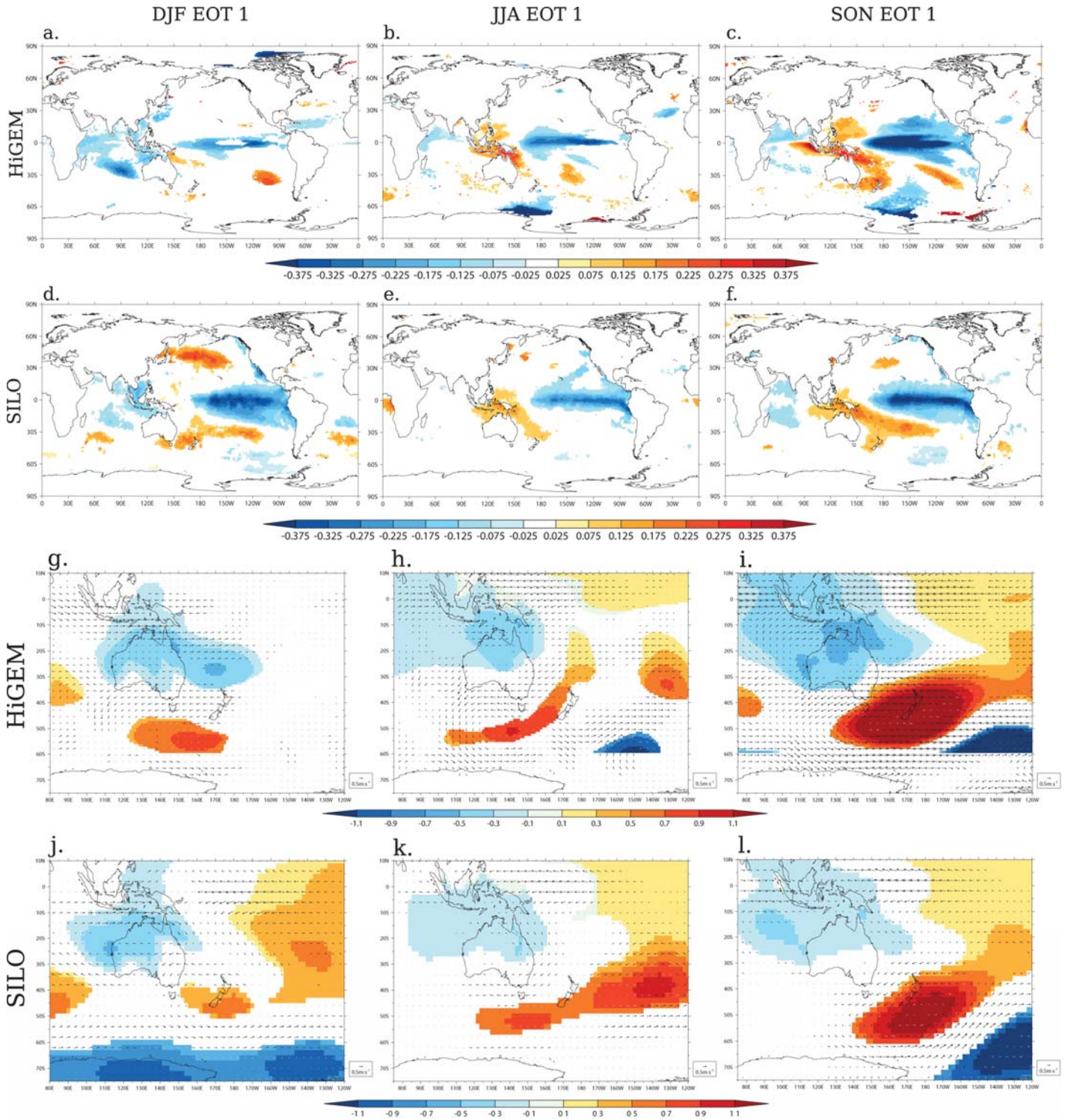

Figure 14: For the three HiGEM EOTs driven by ENSO that have SILO counterparts, the coefficients of linear regression of seasonal-mean (top row) HiGEM SSTs on each HiGEM EOT, (second row) HadISST SSTs on each SILO EOT, (third row) HiGEM MSLP (contours) and 850 hPa winds (vectors) on each HiGEM EOT and (bottom row) 20th Century Reanalysis MSLP (contours) and 850 hPa winds (vectors) on each SILO EOT. Regressions of SST and MSLP are shown only where statistically significant at the 5 per cent level; wind vectors are drawn in black (gray) where significant (not significant) at the 5 per cent level.

6.2.2 Patterns driven by tropical cyclones

Two HiGEM EOTs, DJF EOT 4 (Fig. 11m) and MAM EOT 4 (Fig. 11n), are driven by variations in the number of tracks of tropical cyclones across northern and eastern Queensland. MAM EOT 4, however, is classified as an "extra" HiGEM EOT as it is the non-matching HiGEM EOT—no SILO MAM EOT is driven by tropical cyclones—that explains the least variance in the all-Queensland rainfall (Section 5.2), so it is analysed in Section 5.4. Only HiGEM DJF EOT 4, which matches SILO DJF EOT 2, is discussed further here.

As for SILO DJF EOT 2, HiGEM DJF EOT 4 shows no significant correlations with any of the large-scale drivers analysed here (Table 1). HiGEM DJF EOT 4 does, however, display significant correlations with tropical-cyclone track (Fig. 16a), genesis (Fig. 16b) and lysis (Fig. 16c) densities near the Cape York peninsula. The track and genesis densities suggest that this HiGEM EOT is associated with tropical cyclones that form in the Gulf of Carpentaria, then track southeast across the Cape York peninsula and out into the open ocean. This contrasts with SILO DJF EOT 2, in which cyclones form in the Coral Sea (Fig. 16e) before moving west across Cape York (Fig. 16d) and dying either there or in the Gulf of Carpentaria (Fig. 16f). Decreased 850–200 hPa vertical wind shear across northern and eastern Queensland accompanies high values of both HiGEM DJF EOT 4 (Fig. 16g) and SILO DJF EOT 2 (Fig. 16j); the spatial pattern of wind-shear anomalies is highly consistent between the model and 20CR.

Composites of tropical-cyclone tracks in the 40 seasons when HiGEM DJF EOT 4 is above (Fig. 16h) and below (Fig. 16i) one standard deviation show that seasons of high DJF EOT 4 are clearly associated with an increased number of tropical cyclones making landfall or approaching the Queensland coast. There are very few tracks near Queensland in low DJF EOT 4 seasons, despite having 40 seasons in the composite. The composites compare well with those from SILO DJF EOT 2, using IBTrACS data (Figs. 16k and 16l). Note that there are only six seasons each of the SILO composites, which leads to an obvious discrepancy with the HiGEM composites in the total number of tracks. Even though the tropical cyclones form to the west of Queensland in HiGEM, instead of to the east, HiGEM DJF EOT 4 corresponds well to SILO DJF EOT 2 in the region affected (northern Queensland), the mechanism (tropical cyclones) and the background conditions (reduced vertical wind shear).

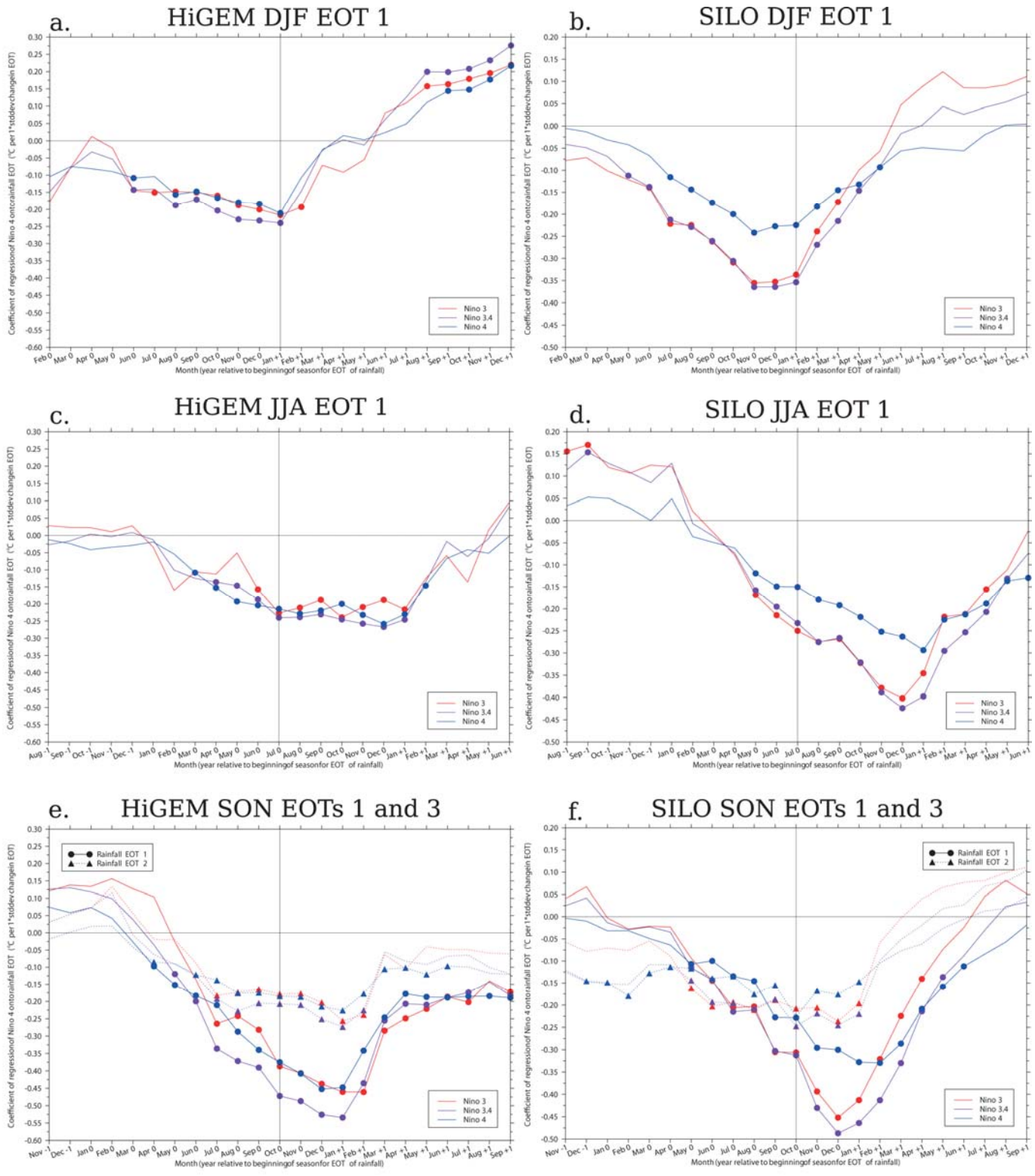

Figure 15: Lead–lag linear regressions of monthly-mean (red line) Niño 3, (purple line) Niño 3.4 and (blue line) Niño 4 SSTs on the time series of (left column) HiGEM EOTs and (right column) SILO EOTs. The solid vertical line gives the centre month of each three-month season. Symbols indicate where the regressions are statistically significant at the 5 per cent level.

6.2.3 Monsoon-driven patterns

HiGEM MAM EOT 1 is the only leading EOT that is not associated with ENSO (Table 1), consistent with SILO MAM EOT 1, which Klingaman (2012b) found was related to the strength of the late-season monsoon and local air–sea interactions. In HiGEM, MAM EOT 1 is linked to a weak enhancement of the monsoon cyclone, with stronger 850 hPa westerly winds and lower mean-sea-level pressures over northern Australia (Fig. 17a). These low-level circulation anomalies are far smaller than in SILO MAM EOT 1 (Fig. 17d), but show similar spatial patterns. HiGEM does not, however, reproduce the warm SST anomalies that were found in HadISST for SILO MAM EOT 1 (Fig. 17e), which supported the hypothesis that this EOT was driven by local air–sea interactions. Instead, HiGEM produces small areas of statistically significant warm anomalies that are almost certainly inconsequential (Fig. 17b). There are considerable increases in synoptic activity in HiGEM (Fig. 17f) - as measured by the standard deviation of MSLP2-10d, as in Klingaman (2012b) - across northern and eastern Australia, including Queensland, that resemble the increases found in 20CR (Fig. 17c). Thus, wet autumns in Queensland in HiGEM are associated with an increase in cyclonic systems crossing the late-season monsoon trough, but the monsoon circulation itself is not enhanced to nearly the same degree as in the corresponding SILO EOT.

The connection between HiGEM MAM EOT 1 and the late-season monsoon is reinforced by regressions of monthly rainfall for March–May onto the EOT time series (Figs. 17g–i). As for SILO MAM EOT 1 (Fig. 17j– l), HiGEM generates nearly all of the rainfall for this EOT in March, when the monsoon trough is typically retreating across northern Australia; the rainfall anomalies in April and May are negligible. Further, the pattern of March rainfall anomalies in HiGEM resembles that from SILO and is consistent with the mean position of the monsoon trough in March, which extends southeast from northern Western Australia through the Northern Territory and across Queensland to the border with New South Wales. Thus, state-wide Queensland rainfall variations in spring are driven by variations in the strength of the late-season monsoon in both observations and HiGEM, although the anomalous low-level cyclonic circulation is far weaker in the latter.

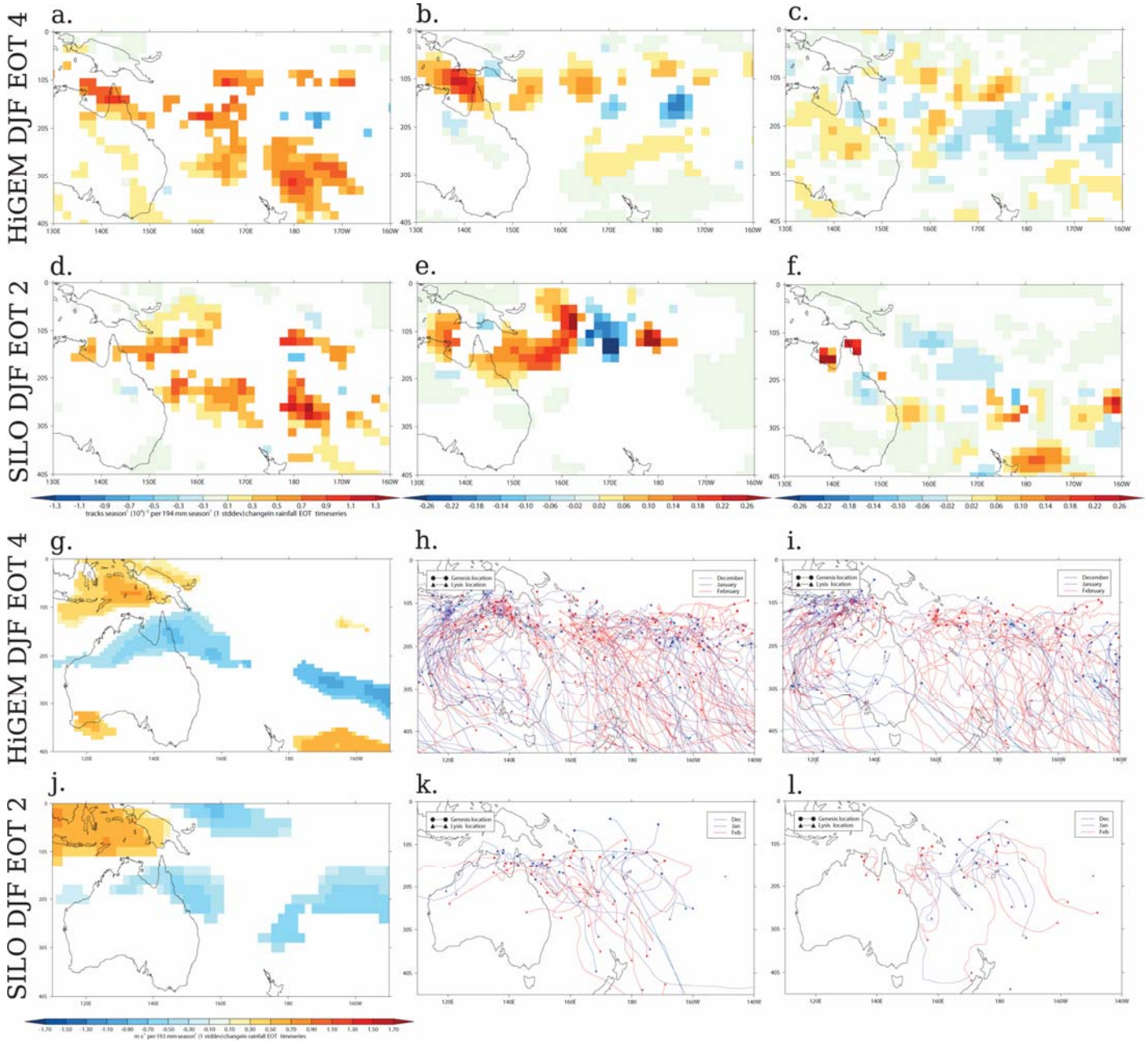

Figure 16: (a–c) Coefficients of linear regression of HiGEM (a) track, (b) genesis and (c) lysis densities (storms season^{-1} 5° spherical cap at each grid point) on HiGEM DJF EOT 4; (d–f) as in (a–c) but for regressions of IBTrACS densities on SILO DJF EOT 2; (g) coefficient of linear regression of seasonal-mean HiGEM 850–200 hPa vertical wind shear on HiGEM DJF EOT 4; (h–i) composites of HiGEM tropical-cyclone tracks in seasons when DJF EOT 4 is (h) above and (i) below one standard deviation; (j–l) as in (g–i) but for 20CR vertical wind shear, IBTrACS tracks and SILO DJF EOT 2. Regression coefficients are shown only where statistically significant at the 5 per cent level.

6.2.4 Patterns driven by local circulations

Four of the SILO EOTs in Klingaman (2012b) were driven by variability in local synoptic patterns and circulations. Of these, three - DJF EOT 3 (Fig. 24c), MAM EOT 2 (Fig. 24f) and JJA EOT 2 (Fig. 24g) - were centred in southern and southeastern Queensland. All displayed decadal or multi-decadal variability, despite having no connection to any large-scale climate mode considered, leading Klingaman (2012b) to conclude that there was natural, independent decadal variability in the weather systems affecting Queensland.

Three of the four locally-driven SILO EOTs have HiGEM counterparts. The spatial pattern of HiGEM DJF EOT 2 (Fig. 11e) strongly resembles that of SILO DJF EOT 3. The 850 hPa circulation over Queensland is also similar to that from 20CR (compare Figs. 18a and 18d), with lower pressures off the east coast and an onshore flow into extreme southern Queensland. HiGEM produces much stronger MSLP and 850 hPa wind anomalies in the Southern Ocean than in 20CR, but the region of highest pressures southwest of New Zealand agrees well with 20CR. The mid-tropospheric (500 hPa) circulation and moisture anomalies are also consistent (compare Figs. 18b and 18e), with an anomalous cyclonic circulation over southeastern Australia and anomalously moist air along the southeastern Queensland coast and just offshore. Finally, there is increased variance in MSLP2–10d along the east coast in both HiGEM (Fig. 18c) and Fig. 18f). Despite overly strong Southern Ocean blocking, HiGEM DJF EOT 2 is clearly very closely related to SILO DJF EOT 3.

HiGEM MAM EOT 2 (Fig. 11f) is shifted east relative to SILO MAM EOT 2, which may be because HiGEM MAM EOT 1 (Fig. 11b) has considerable lower correlations in southeastern Queensland than SILO MAM EOT 1 (Fig. 24b). When the HiGEM MAM EOT 1 pattern was removed from the rainfall time series by linear regression, then, considerable more variance would have remained in southeastern Queensland, relative to the SILO rainfall time series after the removal of SILO MAM EOT 1, favouring southeastern Queensland for the HiGEM MAM EOT 2. The low-level circulation in HiGEM is also shifted, with anomalous cyclone off the east coast of Queensland (Fig. 18g) - similar to DJF EOT 2 - rather than over southeastern Australia as in 20CR (Fig. 18j). The mid-tropospheric pattern are remarkably similar, however (compare Figs. 18h and 18k) with convergence and anomalous high specific humidity along the Queensland coast. HiGEM also produces an increase in $MSLP_{2\text{-}10d}$ variance along the coast, which is slightly shifted east from 20CR, consistent with the shift in the rainfall maximum. Aside from the slight eastward movement of the centre of action in HiGEM, the two MAM EOT patterns are consistent: they affect southern and southeastern Queensland and are driven by anomalous cyclonic activity along the coast and onshore moisture transport.

Coherent variations in southeastern Queensland winter rainfall are described by JJA EOT 2 in HiGEM (Fig. 11g) and SILO (Fig. 24g). Anomalous 850 hPa onshore winds across southeastern Queensland are associated with both the modelled (Fig. 18m) and reanalysis (Fig. 18p) patterns, although HiGEM again exaggerates the spatial extent of the blocking in the Southern Ocean. This leads to positive correlations with blocking in both the 120°–150° E and 150° E–180° bands in HiGEM (Table 1), whereas the SILO JJA EOT 2 is correlated only with 20CR blocking in 150° E–180° only (Table 3). The HiGEM 500 hPa circulation (Fig. 18n) shows an anomalous anticyclone over central Australia that does not appear in 20CR (Fig. 18q), but HiGEM still produces onshore winds and weakly enhanced specific humidity near southeastern Queensland. The strong Southern Ocean blocking in HiGEM reduces $MSLP_{2–10d}$ variance across southeastern Australia (Fig. 18o), which is shifted south from 20CR (Fig. 18r). Still, the key driving mechanism for this mode—the increased blocking activity driving onshore winds—is well-represented in HiGEM.

In each of these three EOTs, HiGEM shows some decadal or multi-decadal variability (Figs. 13b–d). The variability does not persist throughout the integration, as it did throughout the observed record in Klingaman (2012b), but it is promising that HiGEM does produce some significant power on these timescales for these modes. This further strengthens the agreement between HiGEM and SILO in these EOTs.

One SILO EOT driven by local circulations does not have a HiGEM counterpart - JJA EOT 3 - and so is discussed in Section 4.3.2.

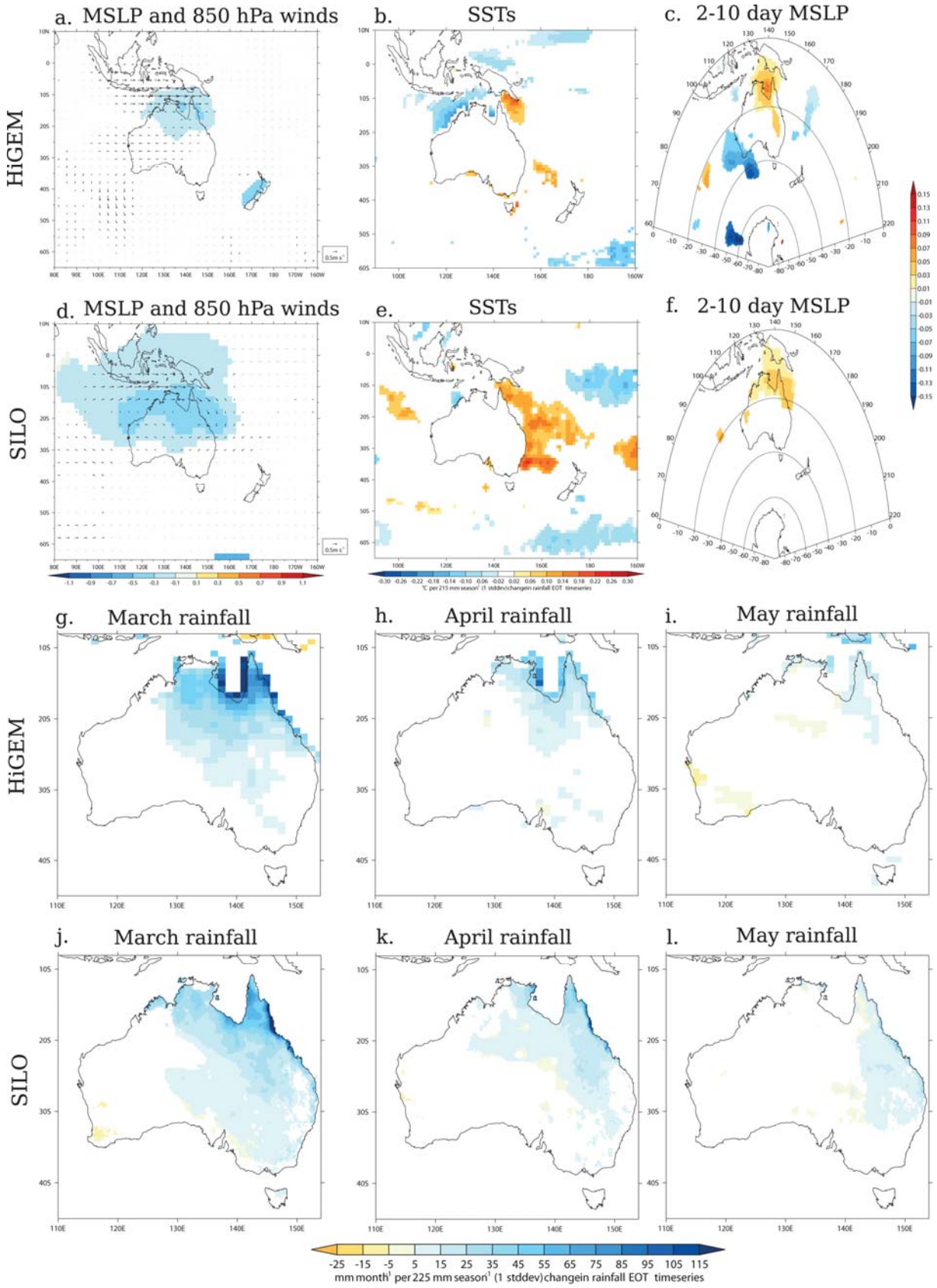

Figure 17: Coefficients of linear regression of (a–c) HiGEM (a) MSLP (contours) and 850 hPa winds (vectors), (b) SST and (c) standard deviation in $MSLP_{2-10d}$ on HiGEM MAM EOT 1; (d–f) as in (a–c) but using 20CR MSLP and HadISST SST on SILO MAMEOT 1; (g–i) HiGEM monthly rainfall for (g) March, (h) April and (i) May on HiGEM MAM EOT 1; (j–l) as in (g–i) but for SILO monthly rainfall on SILO MAM EOT 1.

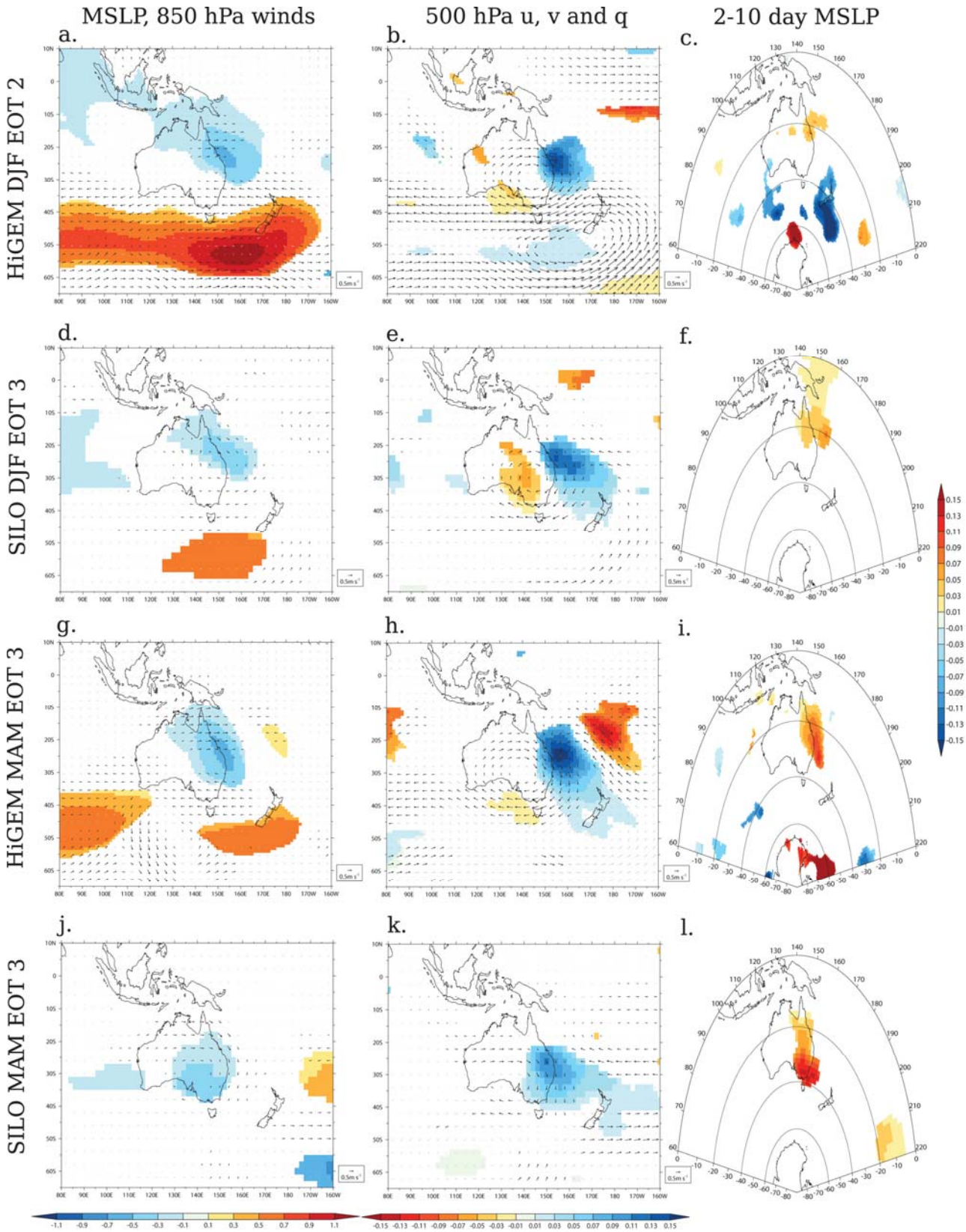

Figure 18: Coefficients of linear regression of (left) MSLP (contours) and 850 hPa winds (vectors); (centre) 500 hPa winds and specific humidity and (right) standard deviation in $MSLP_{2-10d}$ on (a–c) HiGEM DJF EOT 2, (d–f) SILO DJF EOT 3, (g–i) HiGEM MAM EOT 2, (j–l) SILO MAM EOT 2, (m–o) HiGEM JJA EOT 2, (p–r) SILO JJA EOT 2. HiGEM (SILO) EOTs use HiGEM (20CR) fields. Coefficients for MSLP and 500 hPa specific humidity are shown only where statistically significant at 5 per cent; wind vectors are drawn in black (grey) where significant (not significant) at 5 per cent.

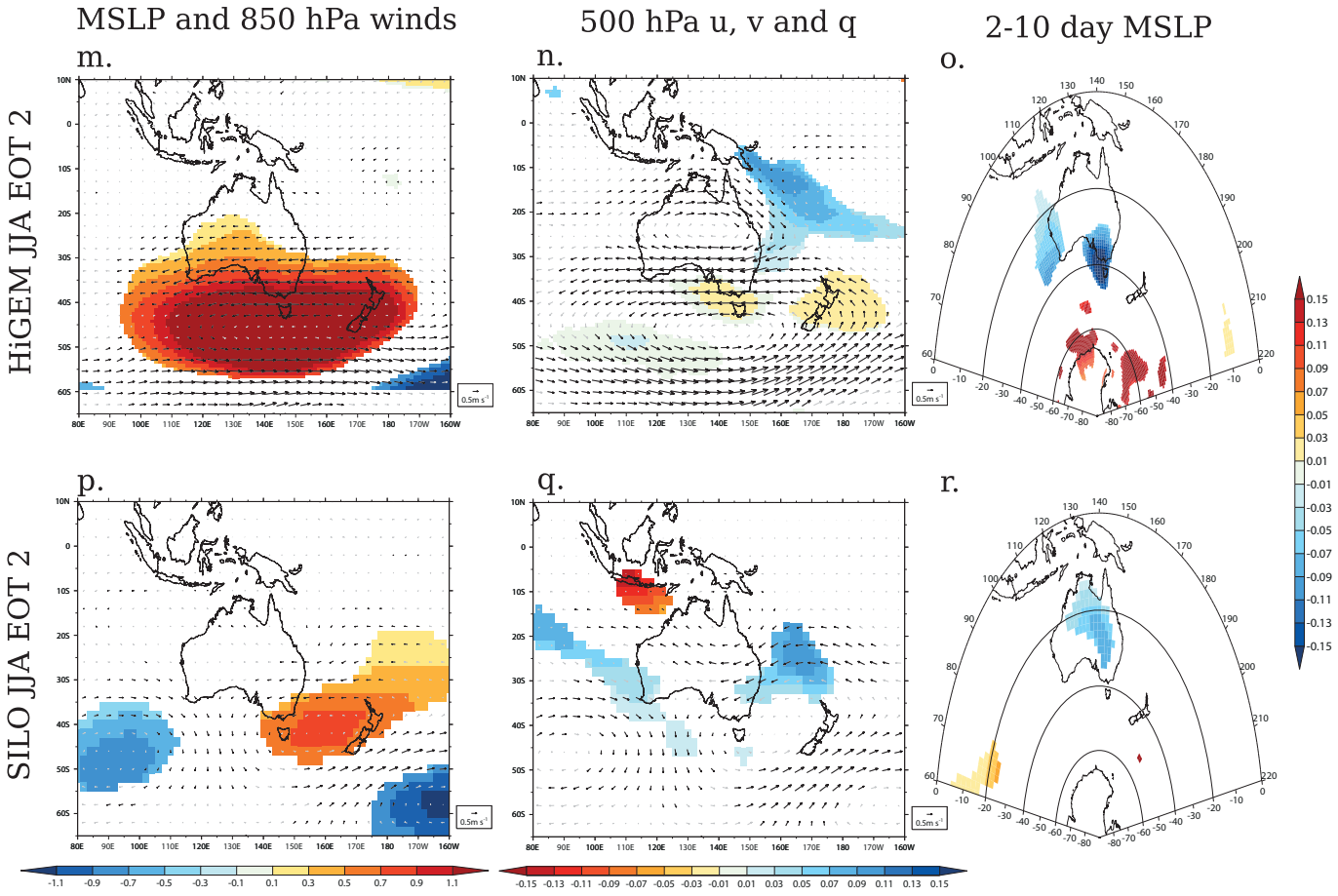

Figure 18 (continued)

6.2.5 SAM-driven patterns

Two HiGEM EOTs demonstrate statistically significant correlations with the SAM: SON EOT 1 and JJA EOT 2 (Table 1). Thus, HiGEM SON EOT 1 is correlated with both the SAM and ENSO (Section 5.2.1), as is its SILO counterpart (Table 3). Both EOTs also show significant partial correlations with the SAM when the influence of ENSO is removed from both the SAM and the EOT time series. MSLP anomalies associated with HiGEM SON EOT 1 show a clear annular signal (Fig. 19a) and are more pronounced than those from 20CR for SILO SON EOT 1 (Fig. 19b), particularly over Antarctica. It is important to note, however, that there are few surface-pressure observations in the Southern Ocean and Antarctica to constrain the 20CR, which may lead to errors in the 20CR in these regions and hence disagreement with the HiGEM MSLP regressions. The HiGEM and SILO EOTs are also positively correlated with blocking activity in the 120–150°E band; the 850 hPa wind regressions in HiGEM (Fig. 14i) show anomalous onshore winds across southern Queensland, consistent with strong anticyclonic activity in the Southern Ocean and the positive SAM phase.

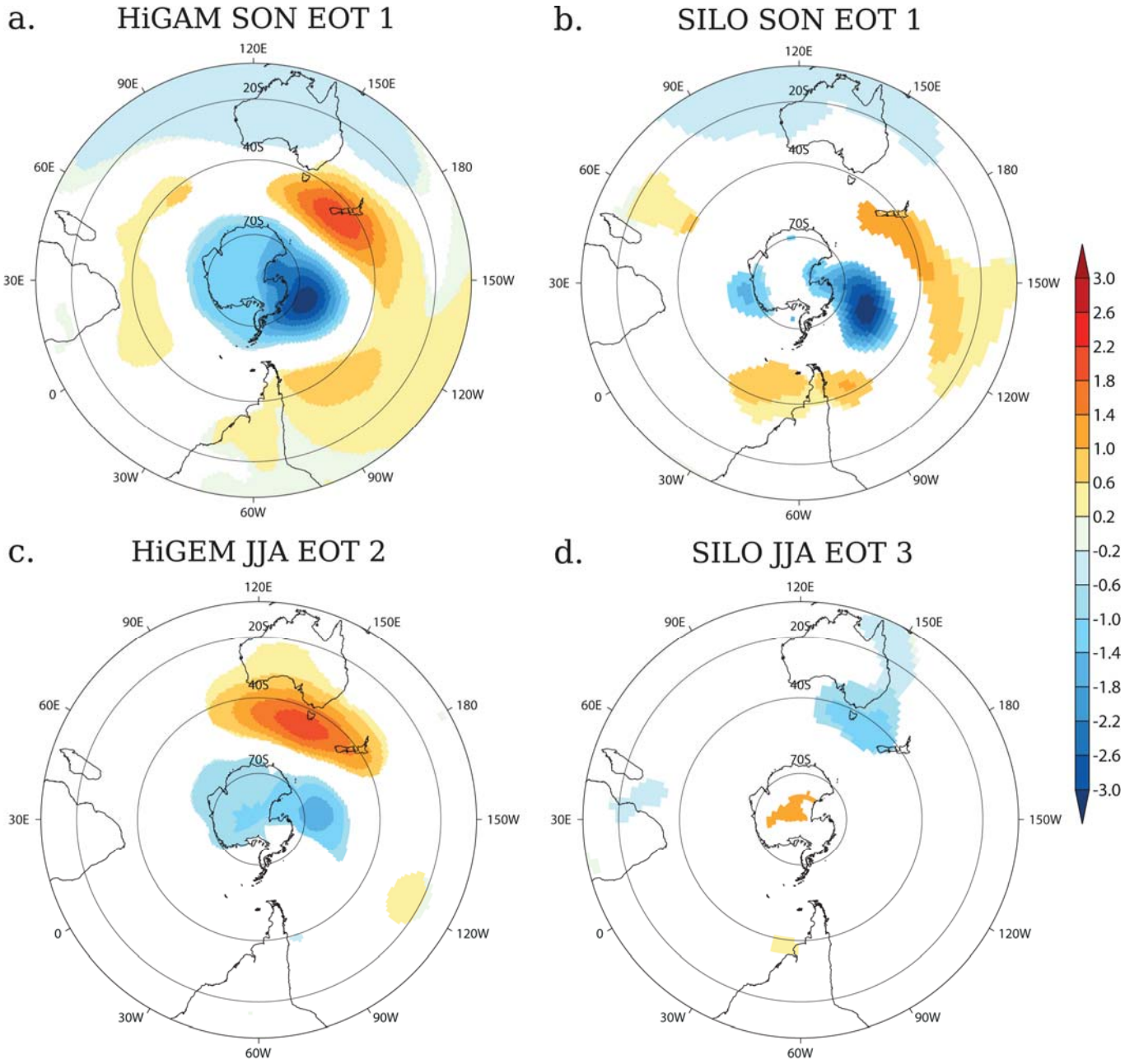

Figure 19: Coefficients of linear regression of (a) HiGEM MSLP on HiGEM SON EOT 1, (b) 20CR MSLP on SILO SON EOT 1, (c) HiGEM MSLP on HiGEM JJA EOT 2 and (d) 20CR MSLP on SILO JJA EOT 3. Regression coefficients are shown only where they are statistically significant at the 5 per cent level.

While HiGEM JJA EOT 2 shows a significant correlation with the SAM, but the MSLP regression pattern fails to show an annular structure at 40°S (Fig. 19c). This EOT was linked to blocking activity and onshore winds in Section 5.2.4; it is likely that the correlation with the SAM arises from the projection of the strong positive MSLP anomalies in the Southern Ocean south of Australia onto the positive SAM phase. Klingaman (2012b) identified similar behaviour, but of the opposite sign, for SILO JJA EOT 3, which showed a negative correlation with the SAM but only regional MSLP anomalies at 40°S (Fig. 19d). That EOT was linked to variability in coastal cyclones and the southward transport of tropical moisture (Table 4). The comparison between HiGEM JJA EOT 2 and SILO EOT 3 is made here not because they are driven by similar mechanisms, but because they demonstrate a statistically significant, but likely physically insignificant correlation with the SAM.

Like SON EOT 1, SILO JJA EOT 1 is correlated with both ENSO and the SAM (Table 3). HiGEM JJA EOT 1 is correlated only with ENSO. Its lack of a connection to the SAM will be considered in Section 5.3.3.

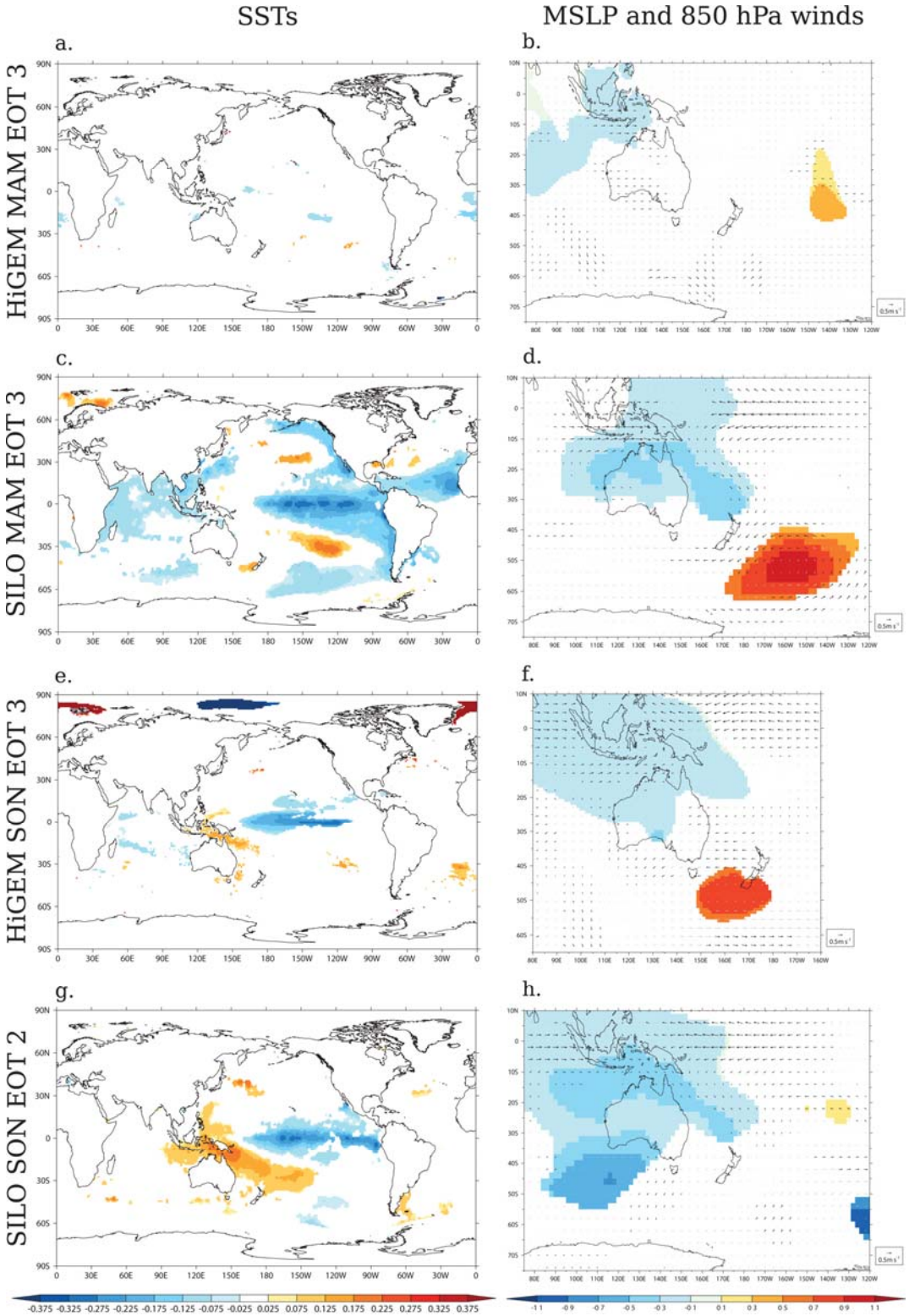

Figure 20: For (a, b) HiGEM MAM EOT 3, (c, d) SILO MAM EOT 3, (e, f) HiGEM SON EOT 3 and (g, h) SILO SON EOT 2, the coefficients of linear regression of (left column) SSTs and (right column) MSLP (contours) and 850 hPa winds (vectors) onto the EOT time series. Regressions for SILO EOTs use HadISST for SSTs and 20CR for MSLP and 850 hPa winds. For SST and MSLP, regressions are shown only where statistically significant at 5 per cent; 850 hPa winds are drawn with black (grey) vectors where statistically significant (not significant) at 5 per cent.

6.3 HiGEM EOTs without SILO counterparts

6.3.1 ENSO-driven patterns

While HiGEM MAM EOT 3 is significantly correlated with Niño 4 SSTs, SST regressions onto the EOT time series show no substantial SST anomalies in the equatorial Pacific (Fig. 20a). This is due to weak inter-annual MAM SST variability in HiGEM in this region (not shown); even though the correlation coefficient exceeds the significance threshold (Table 1), there is very limited SST variability and hence negligible regression coefficients compared to HadISST for SILO MAM EOT 3 (Fig. 20c). The anomalous low-level circulation pattern in HiGEM (Fig. 20b) is also much weaker than observed (Fig. 20d), with no additional convergence near the Maritime Continent, as occurs in SILO MAM EOT 3. Further, the EOTs affect different regions of Queensland, with SILO EOT 3 describing coherent rainfall variability in northern Queensland, while HiGEM EOT 3 describes coherent variations in the southwest and west.

This spatial shift is consistent with the weak instantaneous correlation in HiGEM between Niño 4 and northern Queensland rainfall in MAM (Fig. 5f); HiGEM produces a stronger ENSO teleconnection with southwestern Queensland MAM rainfall, so it is not surprising that the ENSO-linked EOT would be centred there. The low MAM SST variability may be due to the overly bi-annual ENSO in HiGEM, which would lead to weak SST anomalies during the MAM transition season. In reality, some ENSO events persist through the MAM barrier; these are likely responsible for the substantial SST anomalies associated with SILO EOT 3.

Spring is the only season in SILO or HiGEM with two EOTs correlated with Niño 4 SSTs: SON EOTs 1 and 3 in HiGEM and SON EOTs 1 and 2 in SILO. HiGEM SON EOT 1 agreed well with its SILO counterpart and so was discussed in Sections 5.2.1 (for its ENSO connection) and 6.2.5 (for its SAM connection). HiGEM SON EOT 3 and SILO SON EOT 2 are associated with stagnant or decaying ENSO events (Figs. 15e and 15f), as opposed to the SON EOT 1 patterns, which are associated with growing ENSO events that peak in the following DJF. The central Pacific cooling and the anomalously warm SSTs near Australia in HiGEM (Fig. 20e) are similar to the HadISST SST anomalies for SILO SON EOT 2 (Fig. 20g).

The spatial pattern of HiGEM SON EOT 3 (Fig. 11l), however, is displaced far south and west of SILO SON EOT 2 (Fig. 24h). This south-westward displacement also occurred in HiGEM MAM EOT 3, which was also associated with weak and decaying ENSO events. Taken together, these patterns indicate that the ENSO–rainfall teleconnection during weak ENSO events is not represented properly in HiGEM: HiGEM varies the rainfall over the relatively dry interior of southwestern Queensland, rather than the wetter northern tropics. The tropical 850 hPa circulation and MSLP anomalies in HiGEM (Fig. 20f) are also much weaker than in 20CR (Fig. 20h) for this decaying ENSO EOT. HiGEM lacks the anomalous northerlies, and hence the anomalous southward moisture transport, over the Cape York peninsula, consistent with the lack of rainfall anomalies there. HiGEM SON EOT 3 is also associated with Tasman Sea blocking (Table 1), a signal which does not appear in SILO SON EOT 2.

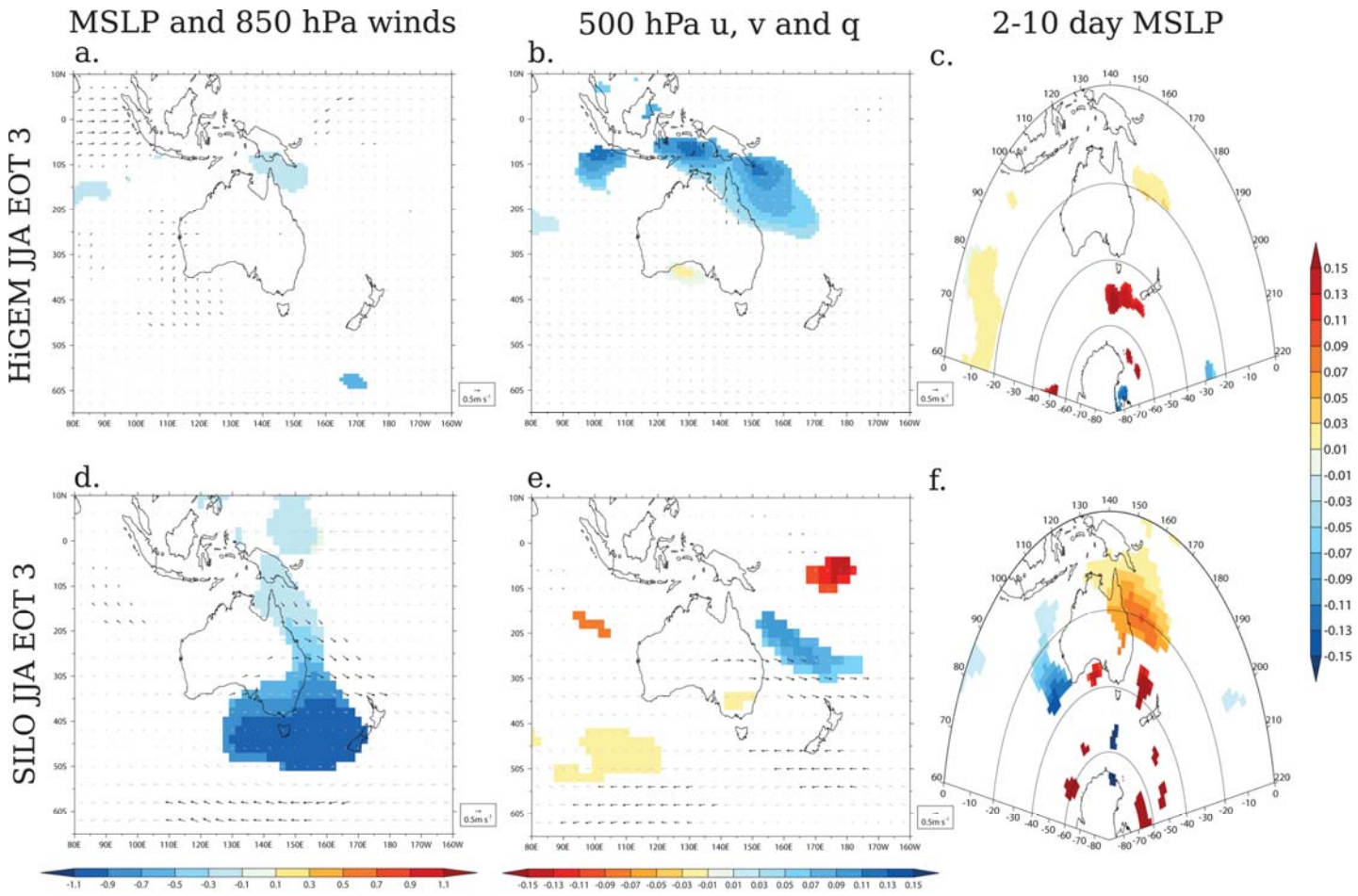

Figure 21: For (a–c) HiGEM JJA EOT 3 and (d–f) SILO JJA EOT 3, the coefficients of linear regression of (a, d) MSLP (contours) and 850 hPa winds (vectors), (b, e) 500 hPa specific humidity (contours) and 500 hPa winds (vectors) and (c, f) the standard deviation in MSLP2–10d. SILO EOTs use 20CR fields for the regressions. MSLP and 500 hPa specific humidity are shown only where the regressions are statistically significant at the 5 per cent level; 850 hPa and 500 hPa wind vectors are drawn in black (grey) where significant (not significant) at 5 per cent.

6.3.2 Patterns driven by local synoptic circulations

While the HiGEM and SILO JJA EOT 3 patterns describe rainfall variability in nearly identical geographical regions (northern and coastal Queensland; compare Figs. 11l and 24l), the local circulation patterns that drive this rainfall variability differ considerably. HiGEM displays few significant low-level circulation anomalies associated with this EOT (Fig. 21a), but has considerable anomalous 500 hPa northerlies across northern Queensland and high positive specific humidity anomalies in wet years (Fig. 21b). This indicates that variations in winter rainfall in northern and coastal Queensland are controlled by the anomalous moisture advection from the tropics. By contrast, Klingaman (2012b) found that SILO JJA EOT 3 was linked to low-level cyclonic anomalies in the Tasman Sea, with anomalous along shore low-level winds (Fig. 21d); there are no significant anomalies in mid-tropospheric tropical moisture or enhanced northerlies in 20CR (Fig. 21e). Further, the SILO EOT was correlated with synoptic activity over much of Queensland and just off the east coast (Fig. 21f), leading Klingaman (2012b) to hypothesise that JJA EOT 3 was driven by coastal cyclones.

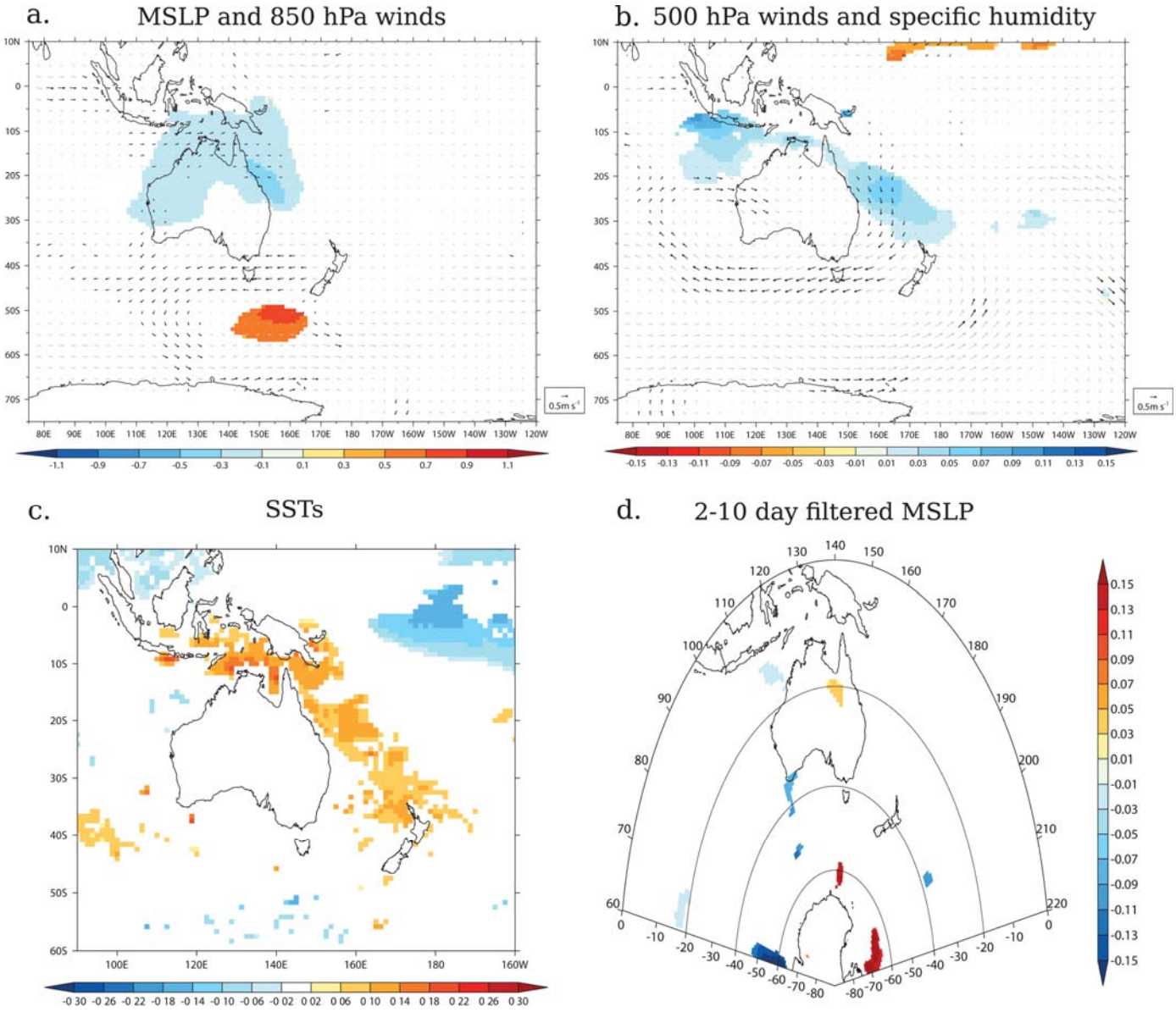

Figure 22: (a–c) As in Fig. 21a–c, but for HiGEM SON EOT 2; (d) coefficients of linear regression of seasonal mean HiGEM SSTs on HiGEM SON EOT 2, with values shown only where significant at the 5 per cent level.

HiGEM JJA EOT 3 is clearly not driven by the same mechanism, as Fig. 21c displays few significant regressions of coastal synoptic activity. Thus, JJA EOT 3 demonstrates the need to carefully examine the physical mechanisms underlying these patterns of rainfall variability in SILO and HiGEM, as similarities in the geographical regions affected alone are insufficient to determine the model's fidelity in simulating the drivers of rainfall.

The spatial pattern of HiGEM SON EOT 2 (Fig. 11h), centred along the eastern coast, does not match any of the leading three SILO EOTs for SON. The HiGEM EOT is correlated with blocking activity in the 150–180° E band with a coefficient barely above the significance threshold (Table 1), but is otherwise unrelated to any other potential driver. The relationship with blocking presents itself as a small area of significant MSLP anomalies and anticyclonic 850 hPa circulation in Figure 22a, but this anomalous circulation does not directly affect Queensland. Instead, coastal Queensland is affected by anomalous 850 hPa westerlies and reduced MSLP, particularly immediately along the coast and the central point of the EOT pattern. Coastal rainfall is also influenced by anomalously moist mid-tropospheric air to the north and east of Australia (Fig. 22b). There are no appreciable changes in synoptic activity over Queensland (Fig. 22c), but the local SSTs are warmer in wet springs along the northern and eastern coasts (Fig. 22d). The similarity in spatial pattern between the MSLP, 500 hPa specific humidity and SST anomalies suggest a role of local air-sea interactions, in which warm SSTs lead to lower

pressures and increased moisture in the atmosphere. As none of the SILO SON EOTs were driven by local air-sea interactions, this HiGEM EOT has no match in observations.

6.3.3 Patterns driven by the SAM

While SILO JJA EOT 1 was correlated with Niño 4 SSTs and the SAM (Table 3), HiGEM JJA EOT 1 is linked with only Niño 4 (Fig. 1). There are few significant extra-tropical MSLP anomalies associated with the HiGEM EOT (Fig. 23a), while the 20CR MSLP anomalies corresponding to the SILO EOT show, for high JJA EOT 1 years, positive anomalies near 40°S and negative anomalies near 65°S, consistent with the positive SAM phase (Fig. 23b). It is important to note that the SAM signal in observations is not purely an extra-tropical ENSO teleconnections, as the partial correlation between rainfall and the SAM, removing the impact of Niño 4 SSTs, is also statistically significant. State-wide rainfall anomalies in winter are controlled by tropical and extra-tropical circulation anomalies in observations, but only the tropical response to ENSO in HiGEM.

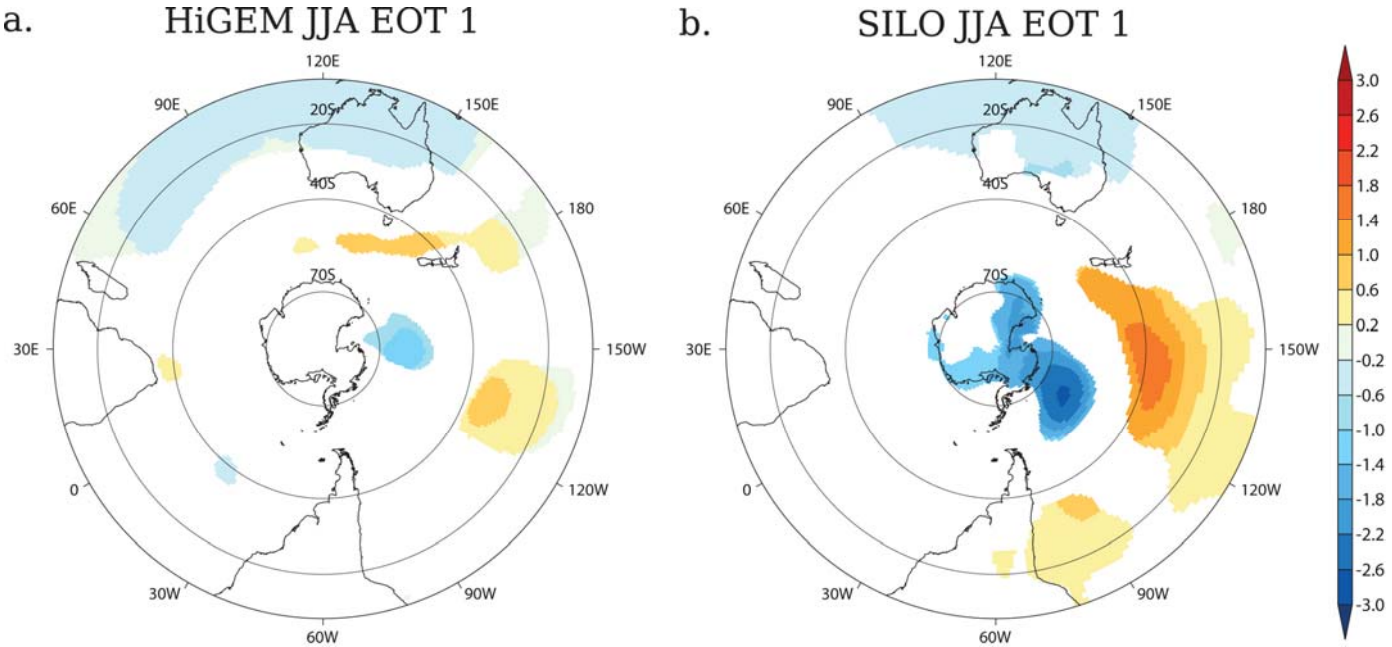

Figure 23: Coefficients of linear regression of (a) HiGEM MSLP on HiGEM JJA EOT 1 and (b) 20CR MSLP on SILO JJA EOT 1. Regression coefficients are shown only where they are statistically significant at the 5 per cent level.

6.4 Additional HiGEM EOTs

This section contains a brief analysis of the "additional" HiGEM EOTs: the HiGEM EOT for each season that does not match one of the three leading SILO EOTs and explains the least variance in the area-averaged Queensland rainfall. These patterns remain because the first four HiGEM EOTs were analysed for each season, but compared to only the first three SILO EOTs.

6.4.1 Patterns driven by tropical cyclones

HiGEM MAM EOT 4 describes coherent rainfall variability in coastal northeastern Queensland (Fig. 11n). It has no significant correlations with any of the potential drivers considered (Table 1), but as for DJF EOT 4, it is associated with substantial variations in tropical-cyclone activity near the Queensland coast. Regressions of track density on MAM EOT 4 show increases in the number of cyclones tracking across northern Queensland in high MAM EOT 4 years (Fig. 24a), with genesis-density regressions indicating more cyclones forming east of Queensland in the Coral Sea and west of Queensland in the Gulf of Carpentaria (Fig. 24b). More cyclone tracks end across northern Queensland in wet autumns along the coast(Fig. 24c), with lower lysis densities just to the south of the region encompassed by this EOT. Vertical windshear is reduced throughout northern Australia in high MAM EOT 4 years (Fig. 24d), which would promote tropical-cyclone development and maintenance. Finally,

composites of cyclone tracks in seasons in which MAM EOT 4 is above (Fig. 24e) and below (Fig. 24f) one standard deviation of its mean emphasise the substantial increase in the number of tropical cyclones near or crossing the Queensland coast in high MAM EOT 4 seasons.

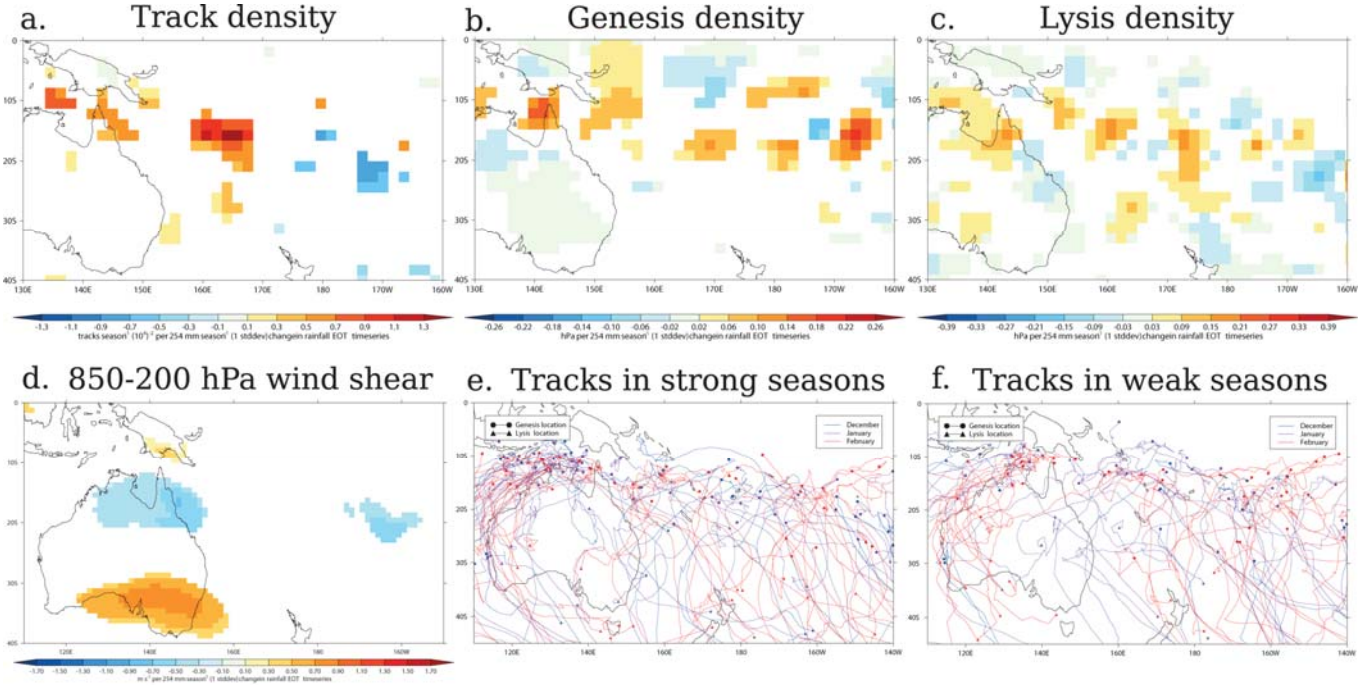

Figure 24: (a–c) As in Figs. 16a–c, but for HiGEM MAM EOT 4; (d–f) as in Figs. 16g–i, but for HiGEM MAM EOT 4.

6.4.2 Patterns driven by local synoptic circulations

Centred in northwestern Queensland, HiGEM DJF EOT 3 (Fig. 11i) also shows no correlation with the potential drivers considered in Table 1. There are no significant anomalies in MSLP or 850 hPa winds associated with this EOT (Fig. 25a), but the 500 hPa and humidity fields (Fig. 25b) reveal a strong tropospheric anomalous cyclone over continental Australia that draws anomalously moist air south from the tropics across western Queensland. There are no substantial changes in synoptic activity near Queensland (Fig. 25c). Thus, it appears that coherent summer rainfall variations in western Queensland in HiGEM are driven by local variations in the strength of the monsoon cyclone that control the advection of tropical moisture across the region at mid-tropospheric levels.

6.4.3 Patterns with no clear driving mechanism

The remaining two HiGEM EOTs - JJA EOT 4 (Fig. 11o) and SON EOT 4 (Fig. 11p), both focused in south-eastern Queensland - have limited significant regression coefficients with all variables considered in this study; these EOTs do not have clear driving mechanisms. Regressions of each against MSLP and 850 hPa winds (Fig. 26a, d), 500 hPa winds and specific humidity (Fig. 26b, e) and the standard deviation in $MSLP_{2\text{-}10d}$ (Fig. 26c, f) are shown for completeness, but the results are inconclusive. It is worth noting that Klingaman (2012) failed to find a driving mechanism for similar south-eastern Queensland EOT in SON-SILO SON EOT 3 - which suggests that coherent south-eastern Queensland rainfall variability in spring, cannot be explained using these analysis techniques. It is also possible that, as these EOTs are artificially constrained to be orthogonal in time, these EOT 4 patterns are unphysical and unrepresentative of rainfall variability in this region.

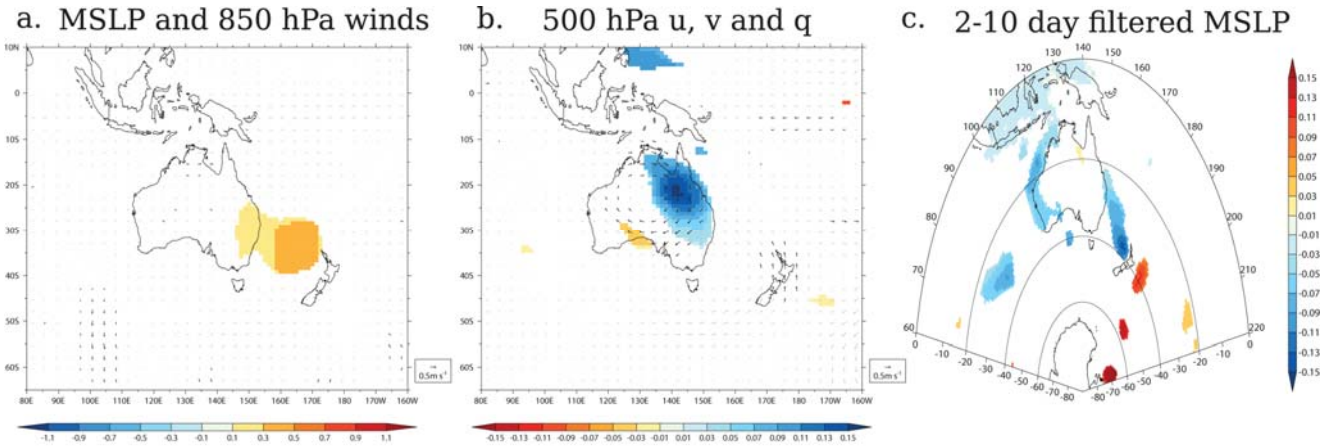

Figure 24: As in Fig. 18a–c, but for HiGEM DJF EOT 3

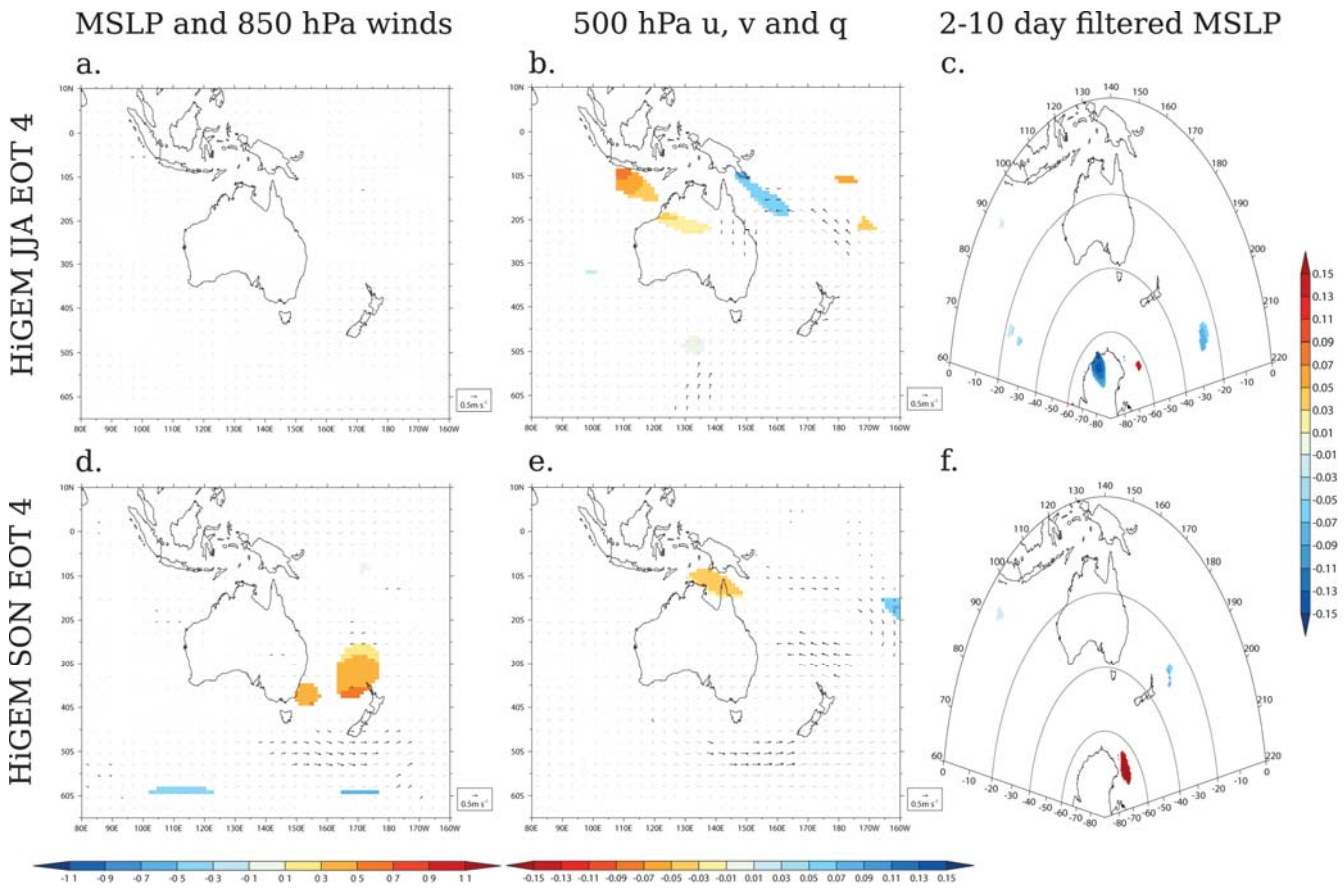

Figure 25: As in Fig. 18a–c, but for (a–c) HiGEM JJA EOT 4 and (d–f) HiGEM SON EOT 4.

7 Summary and conclusions

The ability of the High-resolution Global Environmental Model (HiGEM) to simulate Queensland's rainfall, its natural variability and the drivers of that variability in a 150-year control simulation has been assessed. HiGEM displays a mean-state dry bias over tropical northern Australia and along the eastern coast (Fig. 1c) largely due to deficient rainfall in summer wet season (Fig. 1f); mean rainfall across Australia in the summer wet seasons is well simulated. The presence in HiGEM of considerable DJF wet biases just offshore, combined with the onshore dry biases, suggests that the HIGEM coastal tilting scheme permits ascent and precipitation too far away from the coastline, drying the flow before it can reach land. Aside from northern and eastern Queensland in the summer, HiGEM produces a realistic simulation of seasonal-mean Queensland rainfall.

HiGEM produces near-observed levels of inter-annual variability in rainfall across Australia, for both annual and seasonal rainfall, with slightly strong (weak) variability in northern and eastern (southern and western) Queensland (Fig. 3). The ENSO-Queensland rainfall teleconnection is robust in HiGEM in all seasons, including the seasonal variations in the strength of the correlation (i.e., highest in SON, weakest in MAM) and the spatial pattern of the correlation magnitude (Fig. 5).

The only discrepancies between HiGEM and observations are minor: correlations in northern Australia during the MAM ENSO transition season are weaker than observed, while those in DJF and JJA for eastern Australia are too strong. HiGEM produces reasonable lead–lag relationships between Niño 4 SST anomalies and Queensland rainfall (Fig. 6), except for in February and March when the overly bi-annual nature of ENSO in HiGEM leads to erroneous anti-correlations between rainfall in those months and the ENSO in the remainder of the same calendar year. The observed asymmetric response of Queensland rainfall to Niño 4 SST anomalies—in which the magnitude of rainfall anomalies is correlated with the amplitude of La Niña, but not with the amplitude of El Niño—occurs in HiGEM as well, although the correlation with La Niña is overly dependent upon two large La Niña events in HiGEM that are outside the range of observed events (Fig. 7). HiGEM therefore represents well the inter-annual variations in Queensland's rainfall and its teleconnection with ENSO, the dominant driver of such variability.

On decadal temporal scales, however, HiGEM produces very weak variations in Australian rainfall, relative to the SILO analyses (Fig. 4). This is hypothesised to be due to the lack of an Interdecadal Pacific Oscillation in HiGEM, which in observations has been shown to vary both the total rainfall in Queensland and the strength of the ENSO–Queensland rainfall teleconnection (e.g. Cai et al. 2001; Arblaster et al. 2002; Power et al. 2006; Cai et al. 2010). Despite using a variety of techniques to isolate the IPO in HiGEM—EOFs of 13-year lowpass-filtered SSTs (as in Arblaster et al. 2002), regressions of global 13-year lowpass-filtered SSTs onto 13-year lowpass-filtered SSTs in the equatorial Pacific, and wavelet transforms—little coherent variability between tropical and extra-tropical Pacific SSTs on decadal temporal scales was identified (Fig. 8).

Analysis of the 1000-year control simulation (in 150 year segments) from an older, lower-resolution version of the Hadley Centre coupled model (HadCM3) discovered IPO-like features, demonstrating that such SST variability can exist in a coupled GCM. An extension of the HiGEM control simulation is planned, which would allow a longer period to be discarded from the start of the simulation to account for ocean spin-up. HiGEM lacks natural decadal variability in Queensland rainfall, likely due to the failure of the model to simulate an IPO that resembles observations.

The climatology of tropical-cyclone activity near Queensland in HiGEM compares reasonably well with observations in cyclone tracks and genesis and lysis regions (Fig. 9): there are too many cyclones in HiGEM tracking north of Australia and through the central Pacific, with slightly too few near the east coast of Queensland south of Cairns (Fig. 9c). HiGEM generates most of its cyclones near the Gulf of Carpentaria, consistent with observations (Fig. 9f); differences in lysis density are due to the inclusion of extra-tropical transitions in the HiGEM tracks but not in the observed ones (Fig. 9i). The fidelity of tropical-cyclone variability in HiGEM on all temporal scales (i.e. sub-seasonal to inter-decadal) and the links to known drivers (e.g. ENSO and the Madden–Julian Oscillation) is an active area of research in this project that will be reported separately.

Empirical orthogonal teleconnection analysis of seasonal HiGEM precipitation in Queensland revealed that the model produces many patterns of coherent rainfall variability that are similar to those from SILO, both in their spatial patterns and their underlying physical mechanisms. Table 2 summarises the region each EOT affects, the most likely driving mechanism for each EOT and the SILO EOT to which each HiGEM EOT corresponds, if any.

As in observations (Figs. 26a–d), the leading HiGEM EOTs (Figs. 11a–d) are uni-polar across Queensland and so describe state-wide rainfall variations. In DJF, JJA and SON, these patterns are highly correlated with Niño 4 SST anomalies (Table 1) and associated shifts in tropical circulation patterns, driving cyclonic circulation anomalies and increased cyclonic activity over northern Australia in wet years (Fig. 14), as Klingaman (2012b) found for the SILO EOTs. HiGEM produces weaker variance in Niño 4 SSTs associated with these EOTs, however, than in observations, and the SST anomalies do not peak strongly in DJF (Fig. 15). The leading MAM EOT in HiGEM is related to the strength of the late-season monsoon circulation across Australia, as for SILO, but the anomalous circulation in HiGEM is much weaker than in observations for similar changes in Queensland rainfall (Fig. 17).

Once the leading HiGEM EOTs were removed, the remaining EOTs describe patterns of coherent regional rainfall variations in Queensland. As for the leading patterns, many of these strongly resemble EOTs of SILO rainfall, although the HiGEM EOTs often do not occur in the same order (e.g. HiGEM DJF EOT 2 is similar to SILO DJF EOT 3) due to slight differences in the percentage of variance in the all-Queensland rainfall that each EOT explains. HiGEM performed particularly well for DJF EOTs, despite its mean-state dry bias in this season, which is encouraging the majoritys of Queensland's rainfall occurs during DJF, particularly in the north. HiGEM DJF EOTs 2 and 4 match SILO EOTs 3 and 2, respectively: the former is driven by onshore moisture transport from the combination of low pressure off the coast of Queensland and high pressure in the Tasman Sea (Figs. 18); the latter is caused by variations in tropical-cyclone tracks across the Cape York peninsula (Fig. 16).

By contrast, HiGEM performed poorly for SON EOTs, as only the leading SON EOT has a SILO counterpart. The other HiGEM EOTs were either driven by the same mechanism as in observations but affected the wrong region of Queensland (SON EOT 3) or affected the same region but by the wrong mechanism (SON EOT 2). In MAM and JJA, the leading two HiGEM EOTs matched the leading two SILO EOTs, with the second EOTs being driven by coastal cyclones and Southern Ocean blocking, respectively. Consistent with the overall lack of decadal variability in HiGEM, the EOTs that showed consistent decadal and multi-decadal variability in SILO have little such variability in HiGEM (Fig. 13).

The HiGEM control integration simulates well the mean and inter-annual variability of Queensland's rainfall and its drivers, even capturing the second EOT of SILO rainfall in three of four seasons. The ENSO–Queensland rainfall teleconnection is particularly robust in HiGEM, as are patterns of regional rainfall variability that involve onshore flow along the Queensland coast. Tropical cyclones are also captured well, although drivers of their variability in HiGEM require further investigation. On decadal temporal scales, however, HiGEM performs poorly, most likely due to a weak IPO. These results will inform the analysis of the HiGEM decadal hindcast and prediction simulations for CMIP5, as they indicate which aspects of Queensland's rainfall the model simulates reliably, and which it does not.

Appendix A

SILO EOTs

The spatial patterns (Fig. 27) and time series (Fig. 28) of the three leading EOTs of SILO seasonal rainfall from Klingaman (2012b) are included here for ease of comparison to the EOTs of HiGEM seasonal rainfall, as are the tables of correlations of potential drivers with the SILO EOTs (Table 3) and the summary table listing the mechanism that drives rainfall variability in each EOT (Table 4).

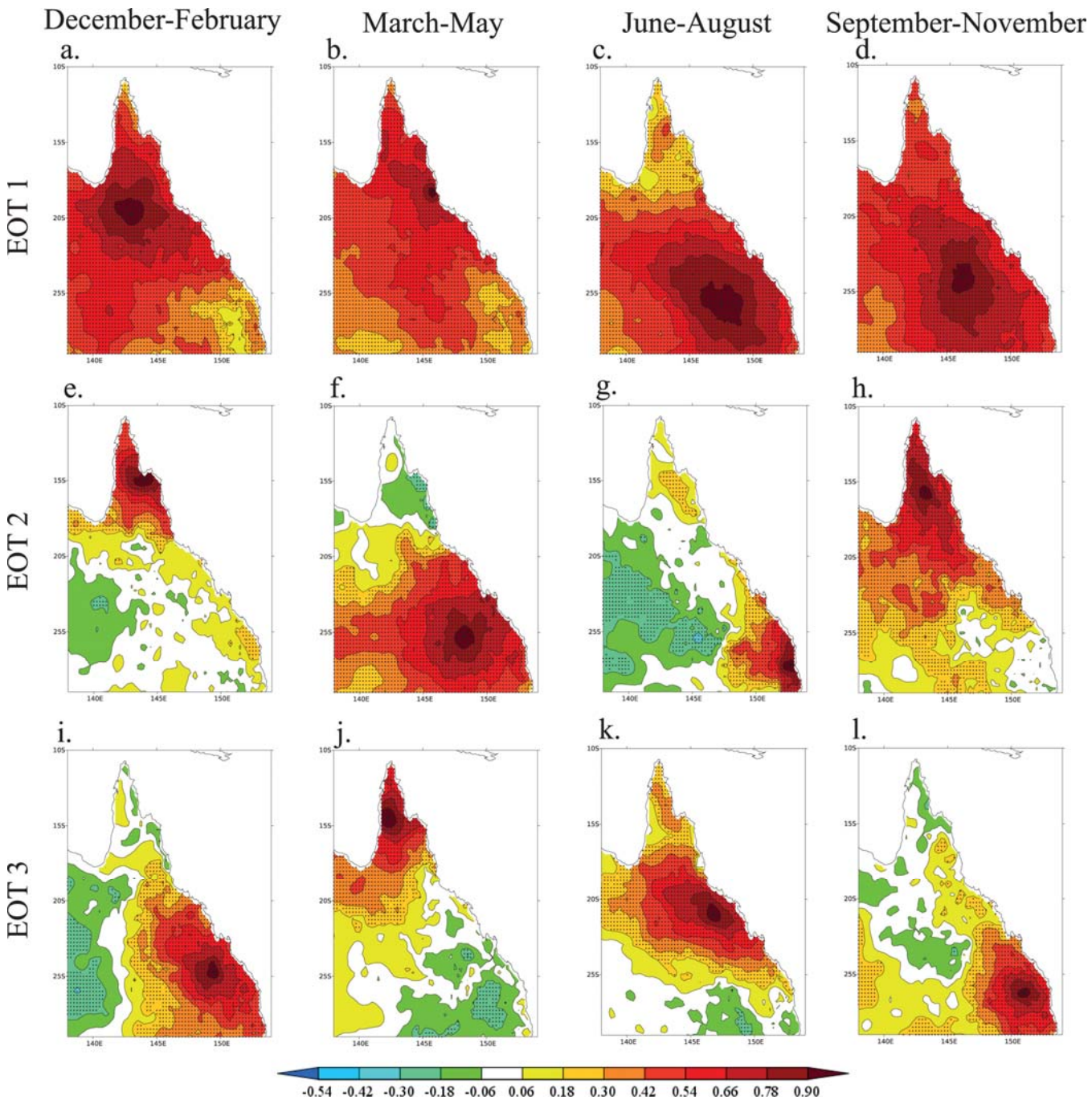

Figure 26: Correlations of the timeseries of seasonal-total (for EOT 1) or residual seasonal-total (EOTs 2 and 3) rainfall at each point with the EOT base point, which is marked with a black triangle. The base point is the one that explains the greatest

variance in the area-average (EOT 1) or the residual area-average (EOTs 2 and 3) Queensland rainfall once any preceding EOTs have been removed by linear regression. Black dots indicate statistically significant correlations at 5 per cent.

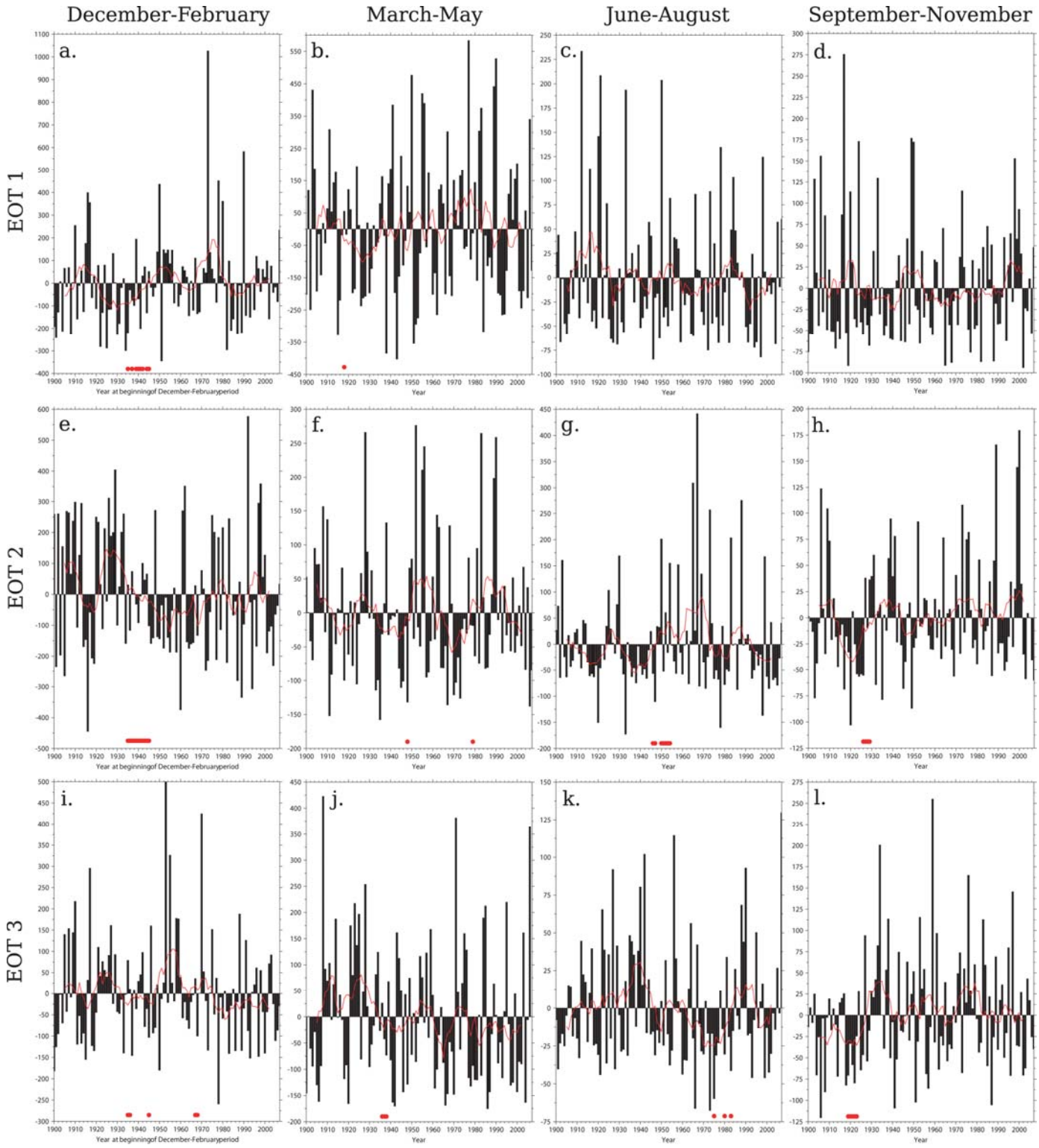

Figure 27: Annual timeseries (black bars) and their 11-year running means (red lines) for each of the EOTs in Fig. 24. Red dots near the horizontal axis indicate when the 31-year centred linear trend is statistically significant at the 5 per cent level. All time series are expressed as anomalies from their mean for ease of interpretation.

Season and EOT	Variance explained	Niño 4	IPO	$B_{120\ 150}$	$B_{150\ 180}$	SAM	$SAM_{\text{Niño 4}}$	IOD	$IOD\|_{\text{Niño 4}}$
December–February									
EOT 1	37.71%	−0.35**	−0.44**	−0.04	0.03	0.28	0.24	0.00	0.11
EOT 2	8.63%	−0.20	−0.02	−0.04	−0.10	0.15	0.12	−0.07	0.05
EOT 3	7.36%	−0.18	−0.22	0.24*	0.12	0.05	0.00	−0.19	−0.12
March–May									
EOT 1	32.17%	−0.17	−0.19	−0.02	−0.16	0.09	0.09	0.07	0.07
EOT 2	13.54%	−0.06	0.01	0.21	−0.15	−0.05	−0.04	0.10	0.10
EOT 3	8.64%	−0.39**	−0.36**	0.05	0.18	0.16	0.15	0.01	0.02
June–August									
EOT 1	45.12%	−0.37**	−0.29*	0.23	0.00	0.25	0.38*	−0.01	−0.07
EOT 2	9.85%	−0.13	−0.11	−0.10	0.26*	0.08	0.11	−0.03	−0.06
EOT 3	6.63%	−0.04	−0.08	0.11	0.19	−0.32*	−0.30*	0.05	0.05
September–November									
EOT 1	41.34%	−0.44**	−0.39**	0.29*	0.18	0.34*	0.32*	−0.25	−0.05
EOT 2	10.91%	−0.30*	−0.25*	0.09	0.12	0.00	−0.06	−0.31*	−0.09
EOT 3	6.80%	−0.12	−0.04	0.26*	0.12	0.31*	0.30*	0.09	0.10

Table 3: For the three leading EOTs of seasonal Queensland rainfall from SILO: the percentage of variance in the area-averaged, seasonal Queensland rainfall explained; the correlations between the EOT time series and Niño 4, the Interdecadal Pacific Oscillation index, the Bureau of Meteorology blocking index longitude-averaged over 120–150°E and 150–180°E, the Southern Annular Mode index and the Indian Ocean Dipole index. For the Southern Annular Mode and the Indian Ocean Dipole, partial correlations with EOT time series are also computed, removing the influence of Niño 4; these are denoted by $|_{\text{Niño 4}}$. An * (**) indicates correlations that are statistically significant at the 5 per cent (1 per cent) level.

Season and EOT	Variance explained	Region affected	Likely driving mechanism
December–February			
EOT 1	37.71%	State-wide	ENSO (peaking) effects on Australian monsoon, modulated by IPO
EOT 2	8.63%	Cape York	Tropical cyclone activity in the Coral Sea
EOT 3	7.36%	Southern	Coastal cyclones and onshore winds
March–May			
EOT 1	32.17%	State-wide	Strength of late-season monsoon, local air–sea interactions
EOT 2	13.54%	Central and southern	Extra-tropical storm track, 500 hPa convergence and moistening
EOT 3	8.64%	Northern	ENSO (decaying) effects on late-season Australian monsoon
June–August			
EOT 1	45.12%	State-wide	ENSO (developing) and SAM influences on extra-tropical storm track
EOT 2	9.85%	Southeastern and western	Blocking in Tasman Sea, driving onshore winds
EOT 3	6.63%	Northern	Coastal cyclones, southward transport of tropical moisture
September–November			
EOT 1	41.34%	State-wide	ENSO (developing) and SAM influences on extra-tropical storm track
EOT 2	10.91%	Northern	ENSO (decaying), southward transport of tropical moisture
EOT 3	6.80%	Southeastern	Unclear, but associations with SAM and Southern Ocean blocking

Table 4: Summary of EOT analysis, giving percentage of variance explained in Queensland-average rainfall, the region of Queensland encompassed by the pattern, and the likely driving mechanism for each EOT.

8 Glossary

Baroclinic - Refers to a condition and type of motion in which pressure is not constant on surfaces of constant density, e.g. internal tides and other internal waves.

Blocking anticyclone - Large scale patterns in the atmospheric pressure field that are nearly stationary, effectively "blocking" or redirecting migratory cyclones. They are also known as blocking highs or blocking anticyclones.

Climate change - A study dealing with variations in climate on many different time scales from decades to millions of years, and the possible causes of such variations. In the most general sense, the term "climate change" encompasses all forms of climatic inconstancy (that is, any differences between long-term statistics of the meteorological elements calculated for different periods but relating to the same area) regardless of their statistical nature or physical causes.

Climate variability - The inherent characteristic of climate which manifests itself in changes of climate with time. The degree of climate variability can be described by the differences between long-term statistics of meteorological elements calculated for different periods.

Cut-off lows - Areas of low surface pressure, closed circulation and intense mid-and upper-tropospheric baroclinic development that form to the south of Australia during periods of atmospheric blocking.

East-coast lows - Areas of closed circulation that form near the eastern coast of Australia south of 20°S and move parallel to the coast. They develop in regions of strong zonal SST gradients and track along the eastern coastline of Australia.

El Niño Southern Oscillation (ENSO) - An irregular oscillation of equatorial Pacific Ocean upper-ocean temperatures, which occurs due to unstable atmosphere–ocean interactions. These ocean-temperature anomalies cause variations in sea-level atmospheric pressure, termed the Southern Oscillation

General Circulation Models (GCM) - Computer models designed to help understand and simulate global and regional climate, in particular the climatic response to changing concentrations of greenhouse gases. GCMs aim to include mathematical descriptions of important physical and chemical processes governing climate, including the role of the atmosphere, land, oceans, and biological processes. The ability to simulate sub-regional climate is determined by the resolution of the model.

Indian Ocean Dipole (IOD) - The difference between sea surface temperature in the western and eastern tropical Indian Oceans. A positive IOD occurs when the western basin is warmer than average and the eastern basin is cool.

Inter-decadal Pacific Oscillation (IPO) - A low-frequency mode of variability in Pacific SSTs; in its positive phase, SSTs are warmer in the East Pacific and in the central equatorial Pacific and cooler in the subtropical and extra-tropical West Pacific in both hemispheres.

Madden-Julian Oscillation (MJO) - A tropical atmospheric phenomena, with a timescale ranging from 40 to 60 days which develops over the Indian Ocean and travels eastwards through the tropics.

Southern Annular Mode (SAM) - The north-south movement of the band of westerly winds south of Australia. SAM is positive when there is a poleward shift of the westerly wind belt and is associated with enhanced spring and summer rainfall in New South Wales and Queensland.

Southern Oscillation - Traditionally defined as normalized sea-level pressure anomalies at Tahiti minus those at Darwin; positive (negative) values correspond to La Niña (El Niño).

Synoptic - Pertaining to a general view of the whole, hence a synoptic variable is one used to describe the state of system over a wide geographical area.

Trade winds - A steady easterly surface winds found in the tropics and blowing towards the equator from the northeast in the northern hemisphere or the southeast in the southern hemisphere, especially at sea. They blow from the tropical high-pressure belts to the low-pressure zone at the equator.

Tropical cyclone - A storm system characterized by a large low-pressure centre and numerous thunderstorms that produce strong winds and heavy rain. Tropical cyclones feed on heat released when moist air rises, resulting in condensation of water vapour contained in the moist air.

Walker Circulation - The east-west movement of the trade winds across the tropical Pacific Ocean, bringing moist surface air to the west with dry air returning along the surface to the east.

9 References

Arblaster, J., G. Meehl, and A. Moore, 2002: Interdecadal modulation of Australian rainfall. Clim. Dynam., 18, 519–531.

Cai, W., P. van Rench, T. Cowan, and A. Sullivan, 2010: Asymmetry in ENSO teleconnection with regional rainfall, its multidecadal variability, and impact. J. Climate, 23, 4944–4955.

Cai, W., P. H. Whetton, and A. B. Pittock, 2001: Fluctuations of the relationship between enso and northeast Australian rainfall. Clim. Dynam., 17, 421–432.

Conkright, M. E., R. A. Locarnini, H. E. Garcia, T. D. O'Brien, T. P.Boyer, C. Stephen, and J. I.Antonov, 2002: World ocean atlas 2001: Objective analyses, data statistics and figures, CD-ROM documentation. Internal Report 17, National Oceanographic Data Centre, 17 pp.

Folland, C. K., D. E. Parker, A. Colman, and R. Washington, 1999: Large scale modes of ocean surface temperature since the late nineteenth century. Beyond El Niño: Decadal and interdecadal climate variability, A. Navarra, Ed., Springer, Berlin, 73–102.

Gordon, C., C. Cooper, C. A. Senior, H. Banks, J. M. Gregory, T.C. Johns, J.F.B. Mitchell, and R.A. Wood, 2000: The simulation of SST, sea ice extents and ocean heat transports in a version of the Hadley Centre coupled model without flux adjustments. Clim. Dynam., 16, 147–168.

Hendon, D., D. Thompson, and M. Wheeler, 2007: Australian rainfall and surface temperature variations associated with the Southern Annular Mode. J. Climate, 20, 2452–2467.

Hodges, K. I., 1996: Spherical nonparametric estimators applied to the UGAMP model integration for AMIP. Mon. Wea. Rev., 124, 2914–2932.

Hopkins, L. C. and G. J. Holland, 1997: Australian heavy-rainfall days and associated east-coast cyclones: 1958–92. J. Climate, 10, 621–635.

Jeffrey, S. J., 2001: Using spatial interpolation to construct a comprehensive archive of Australian climate data. Environ. Model. Softw., 16, 309–330.

Klingaman, N. P., 2012a: A literature survey of key rainfall drivers in Queensland, Australia: Queensland Climate Change Centre of Excellence Research Report: Rainfall in Queensland. Part 1. Department of Environment and Resource Management, Queensland Government, Brisbane, Australia. Available online at www.derm.qld.gov.au

Klingaman, N. P., 2012b: Empirical orthogonal teleconnection analysis of inter-annual variability in Queensland, Australia. Queensland Climate Change Centre of Excellence Research Report: Rainfall in Queensland. Part 3. Department of Environment and Resource Management, Queensland Government, Brisbane, Australia. Available online at www.derm.qld.gov.au

Knapp, K. R., M. C. Kruk, D. H. Levinson, H. J. Diamond, and C. J. Neumann, 2010: The international best track archive for climate stewardship (IBTrACS). Bull. Amer. Meteor. Soc., 91, 363–376.

Marshall, G., 2003: Trends in the southern annual mode from observations and reanalyses. J. Climate, 16, 4134–4143.

Murphy, B. F. and J. Ribbe, 2004: Variability of south-eastern Queensland rainfall and climate indices. Int. J. Climatol., 24, 703–721.

Nicholls, N., 1989: Sea surface temperatures and Australian winter rainfall. J. Climate, 2,965–973.

Power, S., M. Haylock, R. Colman, and X. Wang, 2006: The predictability of interdecadal changes in ENSO activity and ENSO teleconnections. J. Climate, 19, 4755–4771.

Rayner, N. A., D. E. Parker, E. B. Horton, C. K. Folland, L. V. Alexander, D. P. Rowell, E. C. Kent, and A. Kaplan, 2003: Global analyses of sea surface temperature, sea ice and night marine air temperature since the late ineteenth century. J. Geophys. Res., 108, 4407.

Ringer, M. A., G. M. Martin, C. Z. Greeves, T. J. Hinton, P. M. James, V. D. Pope, A. A. Scaife, and R. A. Stratton, 2006: The physical properties of the atmosphere in the new Hadley Centre global environmental model (HadGEM1). Part II: Aspects of variability and regional climate. J. Climate, 19, 1302–1326.

Risbey, J. S., M. J. Pook, P. C. McIntosh, M. C. Wheeler, and H. H. Hendon, 2009: On the remote drivers of rainfall variability in Australia. Mon. Wea. Rev., 137, 3233–3253.

Roberts, M. J. et al., 2009: Impact of resolution on the tropical Pacific circulation in a matrix of coupled models. J. Climate, 22, 2541–2556.

Saji, N. H., B. N. Goswami, P. N. Vinayachandran, and T. Yamagata, 1999: A dipole mode in the tropical Indian Ocean. Nature, 401, 360–363.

Shaffrey, L. et al., 2009: U.K. HiGEM: The new U.K. high-resolution global environment model—Model description and basic evaluation. J. Climate, 22, 1861–1896.

Smith, I., 2004: An assessment of recent trends in Australian rainfall. Aust. Met. Mag., 53, 163–173.

Suppiah, R., K. J. Hennessy, P. H. Whetton, K. McInnes, I. Macadam, J. Bathols, J. Ricketts, and C. M. Page, 2007: Australian climate change projections derived from simulations performed for the IPCC 4th Assessment Report. Aust. Met. Mag., 131–152.

Taylor, K. E., R. J. Stouffer, and G. A. Meehl, 2009: A summary of the CMIP5 experiment design. Available from http://cmip.llnl.gov/cmip5/docs/Taylor CMIP5 design.pdf.

Thompson, D. W. J. and J. M. Wallace, 2000: Annular modes in the extratropical circulation. Part I: Month-to-month variability. J. Climate, 13, 1018–1036.

Thorncroft, C. and K. Hodges, 2001: African easterly wave variability and its relationship to Atlantic tropical cyclone activity. J. Climate, 14, 1166–1179.

Uppala, S. M. et al., 2005: The ERA-40 re-analysis. Q. J. R. Meteorol. Soc., 131, 2961–3012.

Walsh, K. J. E. and J. Syktus, 2003: Simulations of observed interannual variability of tropical cyclone formation east of Australia. Atmos. Sci. Lett., 4, 28–40.